

Flexural buckling of welded austenitic and duplex stainless steel I-section columns

Lu Yang^{a,*}, Menghan Zhao^a, Tak-Ming Chan^b, Fan Shang^a and Dongchen Xu^c

^a*The College of Architecture and Civil Engineering, Beijing University of Technology, Beijing 100124, China*

^b*Department of Civil and Environmental Engineering, The Hong Kong Polytechnic University, Hung Hom, Kowloon, Hong Kong SAR*

^c*Beijing Jiaotong University, Beijing 100044, China*

ABSTRACT

The paper presents an investigation on welded stainless steel I-section columns. In total, 22 experiments on welded I-section columns, including members buckling about major and minor axis, for both austenitic and duplex stainless steel columns were carried out. Specimen cross-sections and lengths were carefully selected to cover a wide range of geometries and non-dimensional slenderness. Measurements were taken on geometry, global initial geometric imperfection, residual stresses and material properties. The experimental results have been supplemented by the finite element simulation. The resulting structural performance data have been used to assess the applicability of the current design provisions from EN 1993-1-4, ASCE 8-02 and AS/NZS 4673 for the design of stainless steel welded-I sections. Results showed that the design provisions from EN 1993-1-4 and AS/NZS 4673 can be conservatively adopted while the ASCE 8-02 provision shows scattered predictions.

Keywords: Austenitic stainless steel; duplex stainless steel; experiments; flexural buckling; numerical analysis; welded I-section columns.

* Corresponding author.

[Tel:+86-10-67392102](tel:+86-10-67392102); [Fax:+86-10-67392102](tel:+86-10-67392102), E-mail: lyang@bjut.edu.cn

1. Introduction

Stainless steel has been adopted in a wide range of structural applications because of its distinguished corrosion resistance, low maintenance cost, superior durability, aesthetic appearance and favorable material properties. There is a variety of grades of stainless steel, characterized through variation in chemical composition and heat treatment. Four main groups can be classified according to the metallurgical structure, namely austenitic, ferritic, duplex (austenitic–ferritic) and martensitic. Two of the most common grades for construction applications are the austenitic and duplex grades. Recent studies of stainless steel focus on its material properties [1-4], residual stress [5-6], flexural behavior [7-9], compression behavior [10-18] and connections [19-21].

Extensive research has been carried out in terms of overall stability behavior of cold-formed thin-walled members, while limited experimental studies are available on axial compression members with welded cross-section. Experimental and numerical research on the interaction of local and overall buckling of cold-formed stainless steel I-columns was conducted by Becque and Rasmussen [11, 14]. Studies of welded sections have also been performed by Yuan *et al.* [16, 17]. Yuan *et al.* [17] tested 28 stainless steel stub columns with welded sections fabricated by shielded metal arc welding (SMAW). Experimental results were compared with the current specifications, including EN1993-1-4 [22], SEI/ASCE 8-02 [23] and AS/NZS 4673 [24]. Assessing the previous research, research on welded I-section axial members are considered to be insufficient and therefore, this paper aims to investigate the flexural buckling behavior of welded austenitic and duplex stainless steel I-section columns. Eleven austenitic and eleven duplex stainless steel column specimens were experimentally examined. Load-strain/displacement histories as well as the failure modes were also recorded. Test results were supplemented by the parallel numerical investigation and the structural performance data were compared against the current design provisions including EN1993-1-4 [22], SEI/ASCE 8-02 [23] and AS/NZS 4673 [24].

2. Material tests, residual stress and geometric imperfection measurements

This section presents the results from the material coupon tests, residual stress and geometric imperfection measurements.

2.1 Specimens and material properties

A total of 22 columns, ten of which were designed for buckling about the major axis while the others for buckling about minor axis, was tested. All specimens were fabricated by SMAW from hot-rolled plates, with water-cutting flanges. Specimen lengths ranged from 1500 mm to 4500 mm. In Table 1, each specimen was identified by a label starting with ‘H’ or ‘I’ to indicate the buckling about minor or major axis respectively. The second part of the label ‘304’/‘2205’ refers to austenitic/duplex stainless steel grade. The third part – ‘1500’ to ‘4500’ refers to the nominal column length. Specimens with ‘B’ possess distinct cross-section, aiming to cover a wider range of slenderness ratio (H304-4000-B and H2205-4000-B). H304-4000-B and H2205-4000-B have same length with H304-4000 and H2205-4000 but with different cross-section. The dimensions of each specimen, including two samples for the residual stress measurements (I304-150 and I2205-150), are summarized in Table 1 with the nomenclature defined in Fig.1. In Table 1, B is the width of the section, H is the height of the section, t_f is the thickness of the flange, b_f is the outstanding width of the flange, t_w is the thickness of web, L is the geometric length, L_t is the distance between rotation centers of two single pole hinges, and $L_t = L + 340$ by considering the dimensions of the hinges. All specimens were Class 1-3 (stocky) sections. Due the anisotropy of stainless steel, the longitudinal direction of the specimens matched with the rolling direction of the constituent plates in the fabrication process.

Tensile coupon tests were carried out in accordance with ISO 6892-1 [25] to evaluate the material characteristics. For each material grade, three coupons, along the rolling direction, were machined from each parent stainless steel plate. The average measured 0.2% proof stress f_y , ultimate stress f_u , modulus of elasticity E_0 and percentage of elongation at fracture and the strain-hardening exponent n are summarized in Table 2. Fig. 2 displays all the measured stress-strain relationships.

2.2 Geometric imperfection and residual stresses measurements

To determine the initial bending value (δ_0) of the specimens, the deviations ($\delta_1, \delta_2, \delta_3$) between section center and the central axis at the quarter-points of the span were recorded. The maximum deviation value was assumed as δ_0 , as shown in Fig.3. The results are summarized in Table 3. In Table 3, the loading eccentricities were determined based on $e = \delta_0 + (e_{ob} + e_{ot})/2$, where e represents the overall geometric initial imperfection, e_{ot} and e_{ob} are the loading eccentricities calculated through the strain measurements near the top (t) and bottom (b) of the specimen respectively. The negative value of e/L in Table 3 indicates that inverse additional bending moments occur.

Residual stresses generated during the welding procedure were measured by the classical sectioning method [16]. The measured magnitude (+ve = tension) and distribution of residual stresses from two typical specimens, I304-150 and I2205-150, are plotted in Fig. 4. Since water cutting was adopted to fabricate the plates, there was barely additional heat input. And hence, compressive stresses are presented at the edge region of flange. Besides, the peak residual tension at edge region of web are lower than that of flange, which may cause by neglect of the released residual stress during cutting process. The variation between the measurements obtained on the interior and exterior surfaces of the sections was relatively small that the residual stress pattern appears biaxially symmetrical. The mean values of these stresses were therefore taken to represent the residual stress state in the sections; this corresponds to the assumption of a uniform strain distribution through the plate thickness. For the I304-150 specimen, the maximum tensile residual stress was 235 MPa ($0.72 f_y$) in the flange, and the maximum compressive residual stress was 183 MPa ($0.57 f_y$). For the I2205-150 specimen, the maximum tensile residual stress was 276 MPa ($0.48 f_y$) in the flange, and the maximum compressive residual stress was 185 MPa ($0.34 f_y$). Simplified residual stress distribution models for stainless steel built-up sections will be devised once further planned residual stress measurements are completed [18]. A regular and continuous form of the residual stress distribution can be seen from Fig.4, while the peak value occurs in the corner.

3. Flexural column buckling tests

3.1 Test configuration

Fig. 5 shows the experimental set up in which a 5000 kN capacity hydraulic testing machine was used to apply the vertical load through knife edge to the specimen. During the initial stages of loading, the load-control mechanism was adopted and displacement-control mechanism was used after reaching the peak load. Similar test set up was also adopted by Chan and Gardner [26]. Once the axial load increased to a certain extent, overall buckling was observed. After reaching the ultimate load, load decreased at a lower rate until the test was stopped due to large lateral displacement.

3.2 Instrumentations

Fig. 6 displays the instrumentation plan of linear variable displacement transducers (LVDT). LVDT-5 and LVDT-6 were placed at mid-length to record the in-plane lateral deflection, while the out-of-plane lateral deflection was measured by LVDT-7. LVDT-3 and LVDT-4 monitored the vertical deflection, i.e. the displacement of the loading point at the bottom of the columns. LVDT-1, LVDT-2 and LVDT-8, LVDT-9 were installed on both sides of each knife edge to measure the end rotation.

Fig. 7 shows the instrumentation plan of strain gauges. As the critical buckling section was anticipated at the mid-height of the column (Section 2), 8 strain gauges (labelled as SG2-1 to SG2-8) were mounted to measure the strain distribution, and 4 others (SG1-1 to SG1-4 or SG3-1 to SG3-4) were attached at both ends of the column (Sections 1 and 3) to aid the evaluation of initial eccentricity.

3.3 Test observations

Overall buckling was identified from the experiments, and the largest horizontal displacement occurred near the mid-height of the columns, while slight torsion was observed for the specimens in

'I' series. Typical flexural buckling modes can be seen in Fig. 8, where I304-2000 and I2205-2000 are illustrated as examples.

3.4 Load-displacement curves

Fig. 9 and Fig. 10 display the vertical and horizontal load-displacement curves for each of the tested austenitic and duplex stainless steel specimens respectively. It shows that the bearing capacity decreases with the increasing slenderness as anticipated. Fig.11 presents the load-end rotation curves for specimens I304-4000 and I2205-4000, which demonstrates the flexibility of the knife edges. Fig. 12 shows the consistent readings between the LVDT-5 and LVDT-6 up to the ultimate load which indicates the specimens were failed by flexural buckling without torsion. Fig. 12 also shows that torsional buckling occurred right after the ultimate load.

Load-out of plane displacement (LVDT-7) of I304-4000 and I2205-4000 are illustrated in Fig. 13. In Fig. 13, the out-of-plane displacement can be barely observed until ultimate load attained. It shows that torsional deformation occurred right after the ultimate load.

3.5 Load-strain histories

Strain readings from SG 2-2, AVG of SG 2-4 and SG 2-5 and SG 2-7 are plotted in Fig. 14 for specimens H304-4000-B, I304-4500, H2205-4000-B and I2205-4500. In Fig. 14, the strain at ultimate load is less than the yielding strain. However, strain at the bottom section exceeds the yielding strain at the end of the tests. It indicates that elastic buckling occurred at the ultimate load while partial section yielded subsequently.

Fig.15 illustrates the buckling strain (strain at the peak load) of different slenderness, where ϵ_y represents yield strain obtained from material tests. The horizontal axis in Fig.15 is non-dimensional slenderness ratio detailed in 5.1. In Fig.15, buckling strain of the stockier specimens exceed the yielding strain while buckling strain of the slenderer columns is below the yielding strain. Generally, the buckling strain decreases with the increase of slenderness.

4. Finite element investigation

A numerical modeling investigation, using the finite element (FE) package ANSYS, was implemented alongside the experimental programme. The objectives of the investigation were to replicate the experimental results and validate the numerical models.

4.1 Numerical modelling methodology

The FE models were established based on the measured geometries of the specimens. BEAM 188, which has been shown to be adaptable for non-linear analysis and perform well in similar study [27] concerning the modelling of axial compression members, was also adopted in this study to mesh welded stainless steel I-section columns. The meshed cross-sectional outline was firstly defined in coordinates and then attached to the model. Details of the mesh are in Fig. 16. The longitudinal mesh size was around 10 cm.

The multiple linear isotropic hardening constitutive model was used to represent the stress-strain response. And the mechanical property parameters in this model were determined by the average tension coupon tests results. The Poisson's ratio was determined as 0.3. Pin-ended support, corresponding to the test configuration, were applied by releasing axial displacement at loading point and Z-axis rotation.

Initial geometric imperfections, inducing during the manufacturing process, were considered in the modelling. The deformation shape of the lowest elastic buckling mode, determined by the linear eigenvalue buckling analysis, is taken as the initial geometric imperfection [28] with the corresponding measured magnitude as shown in Table 3. The simplified residual stress distribution proposed in [6] was added to the integral points of the FE models through 'INISTATE' order, which was carried out based on residual stress measurements and characteristics of self-equilibrium. The amplified initial column buckling mode, simplified residual stress distribution and the simulated results are shown in Fig. 17.

4.2 Validation of models

The applicability of the numerical modelling methodology is assessed by comparing the experimental results with the corresponding numerical data, including the load-deformation curves and buckling strength. The load-vertical and lateral displacement curves of the experiments and simulations for specimens H2205-1500, H2205-3000, I304-2000 and I304-4000 are depicted in Fig.18 and Fig.19. It reveals that the FE simulations are generally in good agreement with the experimental observations. The ratio of the numerical to test buckling strength (P_{FE}/P_{exp}) is listed in Table 4. It is shown that for austenitic stainless steel specimens, the mean value of P_{FE}/P_{exp} is 0.97 while for duplex stainless steel specimens, the mean value of P_{FE}/P_{exp} is 0.98.

5. Buckling resistance of members

In this section, the results of the column buckling experimental and numerical tests are compared with the current column design specifications adopted in Europe, North America, and Australia. ASCE 8-02 and AS/ NZS 4673 for cold-formed stainless steel structures were assessed.

5.1 EN 1993-1-4

In EN 1993-1-4, the nondimensional slenderness is given by

$$\bar{\lambda} = \sqrt{A \cdot f_y / N_{cr}} \quad (1)$$

for Class 1-3 (fully effective) sections

$$\bar{\lambda} = \sqrt{A_e \cdot f_y / N_{cr}} \quad (2)$$

for Class 4 (slender) sections

where N_{cr} is the elastic critical force for the relevant buckling mode based on the gross cross sectional properties.

The overall buckling strength for stainless steel is given by:

$$P_{EC3} = \frac{\chi \cdot A \cdot f_y}{\gamma_{M1}} \quad (3)$$

where P_{EC3} is the design buckling resistance, χ is the reduction factor, γ_{M1} is the resistance partial factor which is taken as 1.1 for stainless steel members to instability, A is the gross section area and f_y is steel yield strength. The reduction factor χ can be obtained from Eq. (4),

$$\chi = \frac{1}{\Phi + \sqrt{\Phi^2 - \bar{\lambda}^2}} \leq 1.0 \quad (4)$$

where $\Phi = 0.5 \left[1 + \alpha(\bar{\lambda} - \bar{\lambda}_0) + \bar{\lambda}^2 \right]$, $\bar{\lambda}_0$ is slenderness limit. Welded I-section specimen buckling about major and minor axis should be designed by different curves according to EN 1993-1-4 [22]. The proposed imperfection impact factor α for specimen buckling about major-axis is 0.49, and $\bar{\lambda}_0$ equals to 0.4, while α for specimen buckling about minor-axis is 0.76, and $\bar{\lambda}_0$ equals to 0.2.

5.2 ASCE 8-02

According to American specification, widths of uniformly compressed elements should be reduced according to its slenderness factor which is given by

$$\lambda_{ASCE} = \left(\frac{1.052}{\sqrt{k}} \right) \left(\frac{w}{t} \right) \left(\sqrt{\frac{f}{E_0}} \right) \quad (5)$$

where k is the plate buckling coefficient taken as 0.5 for unstiffened elements and 4 for stiffened elements, t is the thickness of the uniformly compressed stiffened elements and w is the flat width, for compression members f is taken equal to f_n as determined in Eq(10).

$$B_e = w \quad \text{when } \leq 0.673 \quad (6)$$

$$B_e = \rho w \quad \text{when } > 0.673 \quad (7)$$

where

$$\rho = \frac{1 - 0.22/\lambda}{\lambda} \quad (8)$$

According to ASCE 8-02, the design compressive force is given by

$$P_{ASCE} = \phi_c A_e f_n \quad (9)$$

where ϕ_c is the capacity factor taken as 0.85, A_e is the effective area at buckling stress.

$$f_n = \frac{\pi^2 E_t}{(kl/r)^2} \quad (10)$$

where k is the effective length factor, l is the unbraced length of member and r is the radius of gyration of full unreduced cross section and E_t is given as

$$E_t = \frac{E_0 f_y}{f_y + 0.002 n E_0 \left(\frac{\sigma}{f_y}\right)^{n-1}} \quad (11)$$

5. 3 AS/ NZS 4673

Section reduction is also adopted by Australian specification in the same way with ASCE, the slenderness ratio is given by

$$\lambda_{AS/NZ} = \left(\frac{1.052}{\sqrt{k}}\right) \left(\frac{w}{t}\right) \left(\sqrt{\frac{f}{E_0}}\right) \quad (12)$$

According to AS/NZS 4673, the design compressive force is given by

$$P_{AS/NZ} = \phi_c A_e f_n \quad (13)$$

where ϕ_c is the capacity factor, A_e is the effective area.

For sections not subject to torsional or flexural-torsional buckling,

$$\phi_c = 0.9$$

$$f_n = \frac{f_y}{\phi + \sqrt{\phi^2 - \lambda^2}} \leq f_y \quad (14)$$

where $\phi = \frac{1}{2} (1 + \eta + \lambda^2)$

$$\eta = \alpha ((\lambda - \lambda_1)^\beta - \lambda_0)$$

$$\lambda = \left(\frac{kl}{r}\right) \sqrt{\frac{f_y}{\pi^2 E_0}}$$

where α , λ_1 , β are coefficients reflecting properties for different types of materials according to AS/NZ 4673.

5.4 Discussion

As presented above, calculation method of EN 1993-1-4 is quite different with that of ASCE and AS/NZ. Non-dimensional slenderness ratio is adopted in EN 1993-1-4 while slenderness factor is used to reduce section in ASCE and AS/NZ. According to EN 1993-1-4, effective widths are only used in Class 4 cross-sections to make necessary allowances for reductions in resistance due to the effects of local buckling. Hence gross cross-section has been used in this study. ASCE and AS/NZ methods are roughly the same except for different f_n , which lead to different A_e as shown in Table 5.

Table 6 tabulates the key results of the column tests. Column 2 of Table 6 shows the experimental ultimate loads (P_{exp}) while columns 3 to 5 display the column capacity based on European (P_{EC3}), North American (P_{ASCE}) and Australian ($P_{AS/NZ}$) codes respectively. The final three columns summarize the comparison among P_{exp}/P_{EC3} , P_{exp}/P_{ASCE} , $P_{exp}/P_{AS/NZ}$. Fig. 20 graphically compares the experimental data (denoted by hollow diamond) with the design values based on codes of practice EN 1993-1-4 (denoted by a solid line), ASCE 8-02 (denoted by hollow square), AS/NZS 4673 (denoted by hollow triangle). FE data was also added in the figures (denoted by hollow circle). In Fig 20, the plots were based on EN 1993-1-4 terminology in which the reduction factor χ is plotted against the non-dimensional slenderness $\bar{\lambda}$. As shown in Figs. 19 (a) and (c), for specimens buckling about the major axis, based on the structural performance data, buckling curve for welded open sections (major axis) in EN 1993-1-4 and buckling curves in AS/NZS 4673 can be safely adopted. For specimens buckling about the minor axis, as shown in Figs. 19 (b) and (d), buckling curve for welded open sections (minor axis) in EN 1993-1-4 and buckling curves in AS/NZS 4673

can also be safely adopted. In general, Australian and European specification provides conservative predictions while ASCE predictions are scattered. Generally, ASCE and AS/NZ provide design criteria for the determination of the strength of stainless steel structural members, meaning that effects of welding residual stress are beyond consideration. Therefore, the applicability for welded hot rolled sections is anticipated to verified.

6. Conclusions

A laboratory testing program has been conducted to investigate the flexural buckling of stainless steel welded I-section columns. Eleven austenitic and eleven duplex stainless steel specimens have been reported in this paper. The following findings could be concluded from the results of the experimental investigation:

- In general, overall flexural buckling was observed while torsional deformation occurred in 'I' specimens right after the ultimate load.
- The experimental results have been supplemented by a parallel numerical study. The load-displacement curves and buckling strength of experiments and finite element simulations were compared. Results indicated that the finite element methodology is applicable for future parametric studies.
- With the aid of the structural performance data, the design methods currently adopted in Europe, North America, and Australia for stainless steel column were examined. It can be concluded that EN 1993-1-4 and AS/NZS 4673 show conservative predictions while ASCE 8-02 predictions are scattered which mainly cause by reduction area. It is noted that ASCE 8-02 and AS/NZS 4673 are specific for cold-formed stainless steel structures, and supplemented provisions for welded hot rolled are anticipated.

Acknowledgements

This study is supported by the National Natural Science Foundation of China (Grant No. 51108007) and China Postdoctoral Science Foundation (Grant No. 2013M530500). Their financial support are gratefully acknowledged.

References

- [1] Afshan S, Rossi B, Gardner L. Strength enhancements in cold-formed structural sections — Part I: Material testing. *J Const Steel Res* 2013; 83(4): 177–188.
- [2] Huang Y, Young B. Stress-strain relationship of cold-formed lean duplex stainless steel at elevated temperatures. *J Const Steel Res* 2014; 92(1): 103-113.
- [3] Wang X Q, Z Tao, T. Y. Song. Stress– strain model of austenitic stainless steel after exposure to elevated temperatures. *J Const Steel Res* 2014; 99(8): 129–139.
- [4] Real E, Arrayago I, Mirambell E. Comparative study of analytical expressions for the modelling of stainless steel behavior. *Thin-Walled Struct* 2014; 2–11.
- [5] Jandera M, Machacek J. Residual stress influence on material properties and column behavior of stainless steel SHS. *Thin-Walled Struct* 2014; 83: 12-18.
- [6] Yuan H X, Wang Y Q, Shi Y J, et al. Residual stress distributions in welded stainless steel sections. *Thin-Walled Struct* 2014; 79(2): 38–51.
- [7] Hassanein M F, Silvestre N. Flexural behavior of lean duplex stainless steel girders with slender unstiffened webs. *J Const Steel Res* 2013; 85(5):12–23.
- [8] Shu G P, Zheng B F, Xin L C. A new design method for stainless steel columns subjected to flexural buckling. *Thin-Walled Struct* 2014; (83): 43–51.
- [9] Yang L, Wang Y Q, Gao B. Two calculation methods for buckling reduction factors of stainless steel welded I-section beams. *Thin-Walled Struct* 2014; 128–136.
- [10] Huang Y, Young B. Tests of Pin-ended Cold-formed Lean Duplex Stainless Steel Columns. *J Const Steel Res*, 2013; 82(3): 203-215.

- [11] Zhou F, Chen Y, Young B. Cold-formed High Strength Stainless Steel Cross-sections in Compression Considering Interaction Effects of Constituent Plate Elements. *J Const Steel Res* 2013; 80(1): 32–41.
- [12] Becque J, Rasmussen K J R. Experimental investigation of the interaction of local and overall buckling of stainless steel I-Columns. *J Struct Eng* 2014; 135(11): 1340-1348.
- [13] Afshan S, Gardner L. Experimental study of cold-formed ferritic stainless steel hollow sections. *J Struct Eng* 2013; 139(5): 717-728.
- [14] Becque J, Rasmussen K J R. Numerical investigation of the interaction of local and overall buckling of stainless steel I-Columns. *J Struct Eng* 2009; 135(11): 1349-1356.
- [15] Fan S G, Liu F, Zheng B F. Experimental study on bearing capacity of stainless steel lipped C section stub columns. *Thin-Walled Struct* 2014; 70–84.
- [16] Yuan H X, Wang Y Q, Gardner L, et al. Local–overall interactive buckling of welded stainless steel box section compression members. *Eng Struct* 2014; 67(4): 62–76.
- [17] Yuan H X, Wang Y Q, Shi Y J. Stub column tests on stainless steel built-up sections. *Thin-Walled Struct* 2014; 103–114.
- [18] Zheng B, Hua X, Shu G. Tests of cold-formed and welded stainless steel beam-columns. *J Const Steel Res*, 2015; 111: 1–10.
- [19] Salih E L, Gardner L, Nethercot D A. Numerical investigation of net section failure in stainless steel bolted connections. *J Const Steel Res* 2010; 66(12): 1455-1466.
- [20] Cai Y, Young B. Transient state tests of cold-formed stainless steel single shear bolted connections. *Eng Struct* 2014; 8: 1–9.
- [21] Feng R, Young B. Theoretical analysis of cold-formed stainless steel tubular joints. *Eng Struct* 2015; 83: 99–115.
- [22] European Committee for Standardization. EN ISO 6892-1-2009: Metallic materials Tensile testing- Part 1: Method of test at ambient temperature. Brussels: BSI; 2009.
- [23] American Society of Civil Engineers. SEI/ ASCE 8-02: Specification for the Design of Cold-Formed Stainless Steel Structural Members. Virginia: ASCE; 2002.
- [24] Joint Technical Committee BD- 086. AS/ NZS 4673: Cold- formed Stainless Steel Structures. Sydney: NSW;

2001.

- [25] European Committee for Standardization. EN ISO 6892-1-2009: Metallic materials Tensile testing- Part 1: Method of test at ambient temperature. Brussels: BSI; 2009.
- [26] Chan T M, Gardner L. Flexural Buckling of Elliptical Hollow Section Columns. J Struct Eng 2009; 135(5): 546-557.
- [27] Ban H, Shi G, Shi Y, et al. Overall buckling behavior of 460 MPa high strength steel columns: Experimental investigation and design method[J]. Journal of Constructional Steel Research, 2012, 74(6): 140-150.
- [28] Saliba N, Gardner L. Experimental study of the shear response of lean duplex stainless steel plate girders. Eng Struct 2013; 46(1): 375–391.

Notation

The following symbols are used in this paper:

A	the section area.
A_e	the effective area.
B	the width of the section.
B_e	the effective width.
H	the height of the section.
E_0	the initial elasticity modulus.
E_t	the tangent modulus.
L	the geometric length.
L_t	the distance between rotation centers of two single pole hinges.
L_0	effective length.
N_{cr}	the elastic buckling critical strength based on gross section parameters.
P_{ASCE}	the design buckling strength proposed in the current American steel structure specification.
$P_{AS/NZ}$	the design buckling strength proposed in the current Australian steel structure specification.

P_{EC3}	the design buckling strength proposed in the current European steel structure specification.
P_{FE}	the buckling capacity obtained by numerical analysis.
P_{exp}	the buckling capacity according to the numerical readings.
P_u	the ultimate load.
b_f	the outstanding width of the flange.
e	the total length of the initial geometric imperfection.
e_{0t}	the loading eccentricities at the top of the column
e_{0b}	the loading eccentricities at the bottom of the column
f_u	the ultimate tensile stress.
f_y	the 0.2% proof stress.
k	the plate buckling coefficient.
l	the unbraced length of member.
n	strain-hardening exponents for the compound Ramberg–Osgood model.
r	the radius of gyration of full, unreduced cross section.
t	the thickness of the uniformly compressed stiffened elements.
t_f	the thickness of the flange.
t_w	the thickness of the web.
w	the flat width.
α	the imperfection impact factor.
α, λ_1, β	coefficients reflecting properties for different types of materials
γ_{M1}	the resistance partial factor which is set to 1.1 for architectural construction.
δ	the initial bending value.
λ	slenderness ratio.
$\bar{\lambda}$	the non- dimensional slenderness.
$\bar{\lambda}_0$	the limiting slenderness.
ϕ_c	the capacity factor.
χ	the reduction factor.

Table 1

Measured dimensions of specimens

Specimen	B (mm)	H (mm)	t_f (mm)	t_w (mm)	b_f (mm)	L (mm)	L_t (mm)
H304-1500	149.1	150.2	10.00	6.00	70.7	1535.7	1875.7
H304-2000	149.1	150.1	10.00	6.00	71.8	2037.4	2377.4
H304-3000	149.6	150.0	10.00	6.00	72.8	3043.7	3383.7
H304-3500	149.6	149.6	10.00	6.00	72.8	3537.3	3877.3
H304-4000	149.4	150.0	10.00	6.00	72.9	4036.8	4376.8
H304-4000-B	119.1	149.7	10.00	6.00	57.5	4029.1	4369.1
I304-2000	149.2	149.8	10.00	6.00	73.1	2037.1	2377.1
I304-3000	149.3	150.3	10.00	6.00	73.7	3033.5	3373.5
I304-3500	149.5	110.4	10.00	6.00	72.0	3534.8	3874.8
I304-4000	150.0	150.2	10.00	6.00	73.2	4034.4	4374.4
I304-4500	120.1	100.0	10.00	6.00	57.4	4532.9	4872.9
H2205-1500	149.9	150.8	10.20	6.00	73.1	1539.3	1879.3
H2205-2000	150.0	150.4	10.20	6.00	72.6	2038.9	2378.9
H2205-3000	149.7	150.3	10.20	6.00	72.7	3041.4	3381.4
H2205-3500	151.2	150.1	10.20	6.00	72.7	3540.8	3880.8
H2205-4000	149.9	150.1	10.20	6.00	71.3	4035.5	4375.5
H2205-4000-B	120.1	150.3	10.20	6.00	56.7	4038.2	4378.2
I2205-2000	150.7	150.3	10.20	6.00	73.4	2040.2	2380.2
I2205-3000	149.9	150.0	10.20	6.00	73.4	3037.2	3377.2
I2205-3500	150.9	150.4	10.20	6.00	72.7	3543.6	3883.68
I2205-4000	148.5	150.1	10.20	6.00	71.8	4038.7	4378.7
I2205-4500	150.4	110.8	10.20	6.00	72.4	4536.0	4876.0
I304-150	149.5	150.1	10.00	6.00	70.3	449.6	—
I2205-150	149.0	150.1	10.20	6.00	70.3	449.4	—

Table 2

Material properties along the rolling direction

Grade	t (mm)	E_0 (MPa)	f_y (MPa)	f_u (MPa)	Elongation at fracture (%)	n
Austenitic	6.00	182300	282	696	58.1	6.5
	10.00	198700	321	660		6.0
Duplex	6.00	191900	553	798	35.0	7.0
	10.20	190400	547	775		6.4

Table 3

Measured initial bending of specimens

Specimen	Initial bending (mm)				Loading eccentricity (mm)		e/L
	δ_1	δ_2	δ_3	δ_0	e_{0b}	e_{0t}	
H304-1500	0.216	0.029	0.294	0.294	-9.00	-3.80	-1/246
H304-2000	0.072	0.034	0.102	0.102	-14.66	-14.84	-1/137
H304-3000	0.069	0.035	0.149	0.149	-2.74	-4.83	-1/826
H304-3500	0.105	0.237	0.181	0.237	9.96	48.65	1/118
H304-4000	0.137	0.055	0.185	0.185	-5.70	55.20	1/163
H304-4000-B	0.052	0.129	0.103	0.129	-2.58	-18.50	-1/385
I304-2000	1.841	3.223	1.852	3.223	-2.27	-5.03	1/291
I304-3000	0.005	0.232	0.448	0.448	0.79	4.78	1/926
I304-3500	0.226	0.399	0.007	0.399	-4.60	-3.66	1/775
I304-4000	0.207	5.042	0.234	5.042	0.97	-3.68	1/1087
I304-4500	0.223	0.162	0.115	0.223	-0.79	-1.42	1/5263
H2205-1500	0.599	0.389	0.533	0.599	5.34	10.43	1/181
H2205-2000	0.327	0.010	0.373	0.373	5.70	2.16	1/474
H2205-3000	0.329	0.428	0.616	0.616	12.38	66.53	1/76
H2205-3500	0.076	0.315	0.353	0.353	-55.39	-24.34	1/90
H2205-4000	0.380	0.196	0.258	0.380	10.85	-4.45	1/1123
H2205-4000-B	0.712	1.028	0.027	1.028	11.87	-39.30	-1/318
I2205-2000	0.378	0.703	0.281	0.703	-3.23	19.23	1/234
I2205-3000	0.135	0.177	0.616	0.616	-3.14	8.52	1/917
I2205-3500	0.267	0.256	0.267	0.267	-3.35	5.32	1/2857
I2205-4000	0.242	0.259	0.216	0.259	-8.56	7.09	-1/8333
I2205-4500	0.364	0.160	0.450	0.450	-0.60	1.41	1/5263

Table 4

Comparison between experimental and simulation results

Specimens	$\bar{\lambda}$	P_{exp} (kN)	P_{FE} (kN)	P_{FE}/P_{exp}
H304-1500	0.623	956	882	0.92
H304-2000	0.789	821	769	0.94
H304-3000	1.117	599	533	0.89
H304-3500	1.283	490	466	0.95
H304-4000	1.451	392	372	0.95
H304-4000-B	1.861	262	245	0.94
I304-2000	0.469	1000	1006	1.01
I304-3000	0.663	914	874	0.96
I304-3500	1.041	608	643	1.06
I304-4000	0.862	691	724	1.05
I304-4500	1.470	282	296	1.05
			AVG	0.97
			COV	0.0033
H2205-1500	0.830	1470	1474	1.00
H2205-2000	1.050	1128	1100	0.98
H2205-3000	1.496	751	720	0.96
H2205-3500	1.698	677	623	0.92
H2205-4000	1.932	524	511	0.98
H2205-4000-B	2.473	321	302	0.94
I2205-2000	0.626	1705	1792	1.05
I2205-3000	0.891	1366	1360	0.99
I2205-3500	1.021	1228	1235	1.01
I2205-4000	1.155	1065	1080	1.01
I2205-4500	1.750	619	606	0.98
			AVG	0.98
			COV	0.0013

Table 5

Effective area values for all three design codes

Specimen	$A_{EC3}(\text{mm}^2)$	$A_{ASCE}(\text{mm}^2)$	$A_{AS/NZ}(\text{mm}^2)$
H304-1500	3779	3448	3610
H304-2000	3779	3547	3744
H304-3000	3779	3735	3779
H304-3500	3779	3779	3779
H304-4000	3779	3779	3779
H304-4000-B	3180	3180	3180
I304-2000	3779	3348	3468
I304-3000	3779	3472	3644
I304-3500	3540	3450	3540
I304-4000	3779	3586	3779
I304-4500	2880	2880	2880
H2205-1500	3779	3060	3160
H2205-2000	3779	3187	3334
H2205-3000	3779	3534	3706
H2205-3500	3779	3718	3779
H2205-4000	3779	3779	3779
H2205-4000-B	3180	3180	3180
I2205-2000	3779	2540	3024
I2205-3000	3779	2942	3210
I2205-3500	3779	3048	3311
I2205-4000	3779	3068	3422
I2205-4500	3540	3516	3540

*Note: Gross areas are adopted in EN 1993-1-4 for all specimens belong to Class 1-3 sections. A_{ASCE} and $A_{AS/NZ}$ are reduced areas.

Table 6

Buckling capacity calculated by experiments and specifications

Specimen	$P_{exp}(kN)$	$P_{EC3}(kN)$	$P_{ASCE}(kN)$	$P_{AS/NZ}(kN)$	$\frac{P_{exp}}{P_{EC3}}$	$\frac{P_{exp}}{P_{ASCE}}$	$\frac{P_{exp}}{P_{AS/NZ}}$
H304-1500	956	742	807	704	1.29	1.19	1.36
H304-2000	821	626	718	597	1.31	1.14	1.38
H304-3000	599	441	570	433	1.36	1.05	1.38
H304-3500	490	369	496	368	1.33	0.99	1.33
H304-4000	392	311	421	314	1.26	0.93	1.25
H304-4000-B	262	177	228	183	1.48	1.15	1.43
I304-2000	1000	920	908	835	1.09	1.10	1.20
I304-3000	914	800	784	677	1.14	1.17	1.35
I304-3500	608	522	565	437	1.16	1.08	1.39
I304-4000	691	669	685	556	1.03	1.01	1.24
I304-4500	282	267	314	235	1.06	0.90	1.20
				AVG	1.23	1.06	1.32
				COV	0.0183	0.0086	0.0061
H2205-1500	1470	1231	1321	1232	1.19	1.11	1.19
H2205-2000	1128	979	1135	1011	1.15	0.99	1.12
H2205-3000	751	603	754	648	1.24	1.00	1.16
H2205-3500	677	497	603	532	1.36	1.12	1.27
H2205-4000	524	398	470	429	1.32	1.12	1.22
H2205-4000-B	321	217	242	233	1.48	1.33	1.38
I2205-2000	1705	1478	1512	1461	1.15	1.13	1.17
I2205-3000	1366	1157	1269	1169	1.18	1.08	1.17
I2205-3500	1228	1015	1159	1039	1.21	1.06	1.18
I2205-4000	1065	865	1047	913	1.23	1.02	1.17
I2205-4500	619	442	533	474	1.40	1.16	1.31
				AVG	1.26	1.10	1.21
				COV	0.0110	0.0080	0.0054

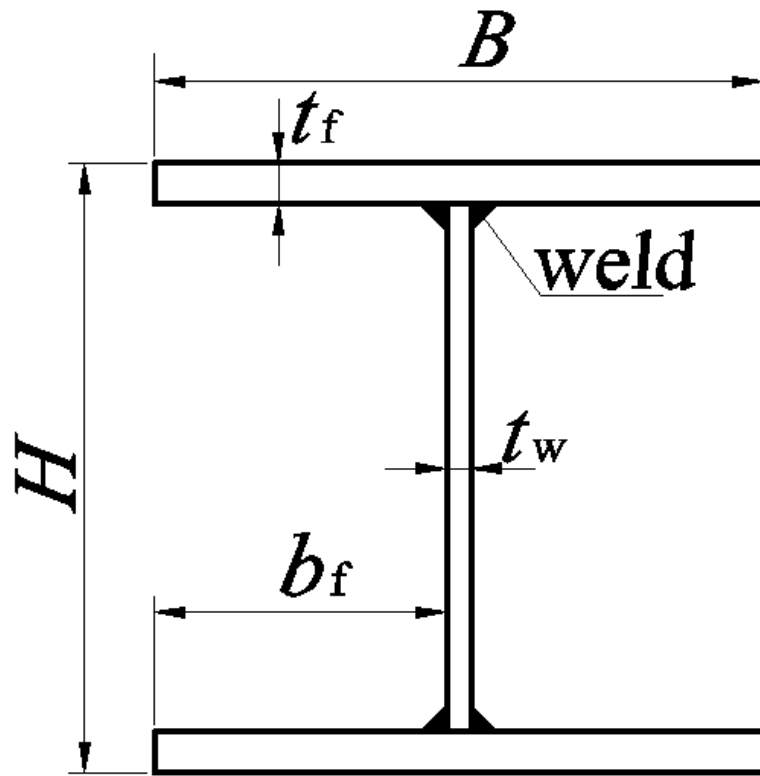
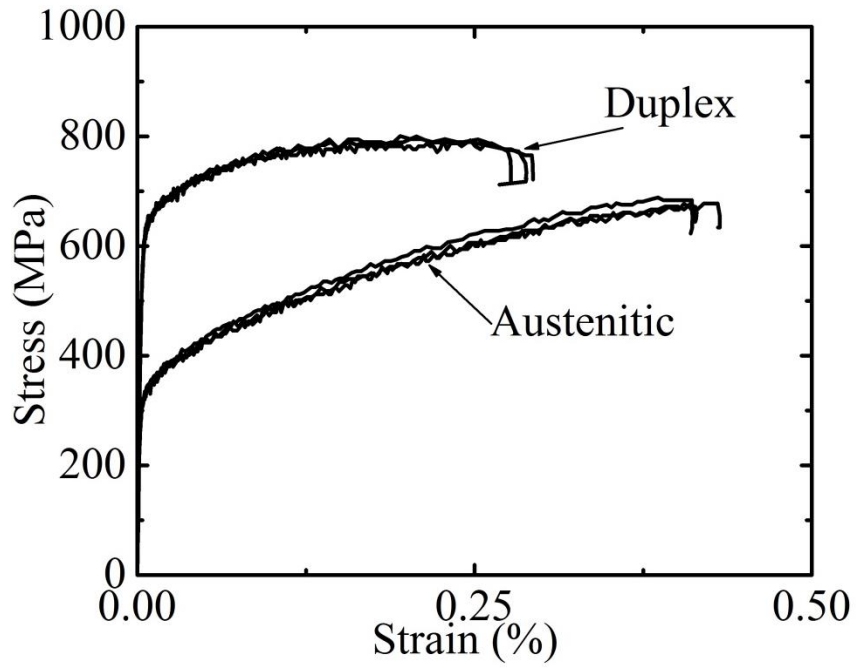
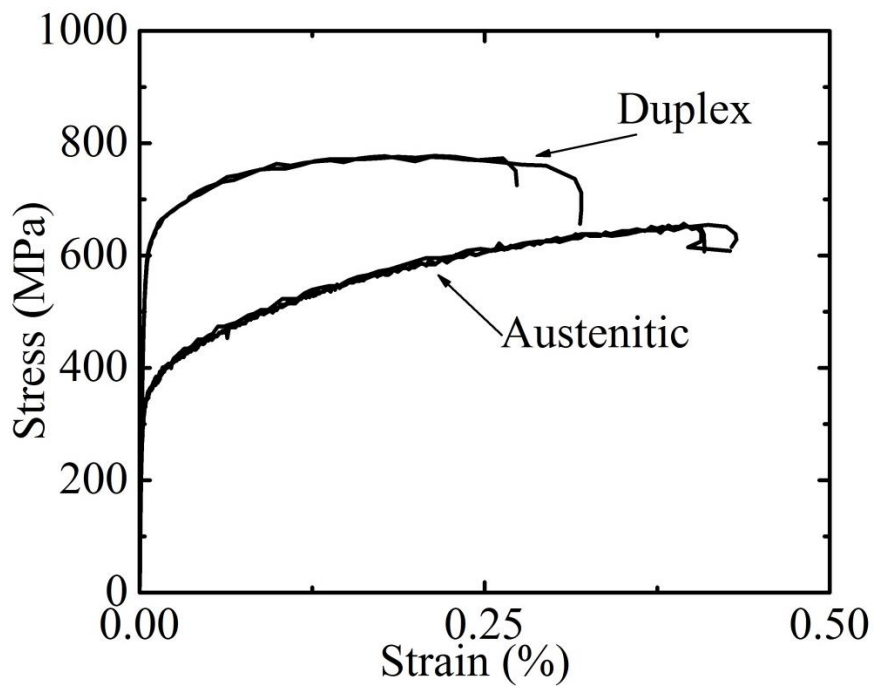


Fig.1. Cross-section notations



(a) 6 mm plates



(b) 10 mm plates

Fig.2. Material stress-strain curves

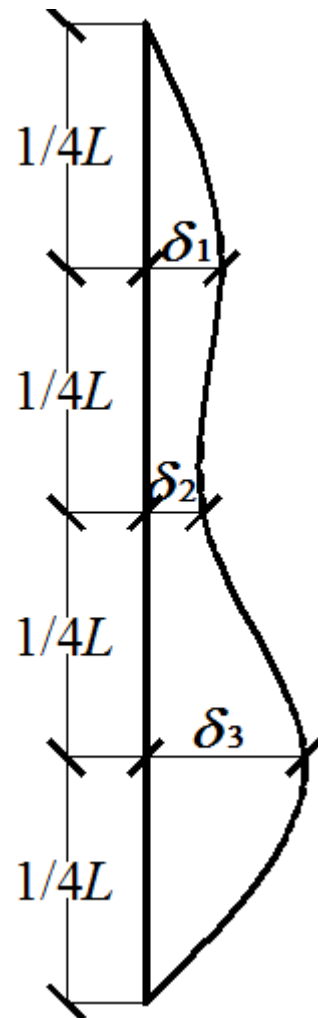


Fig.3. Illustration of initial bending measurement

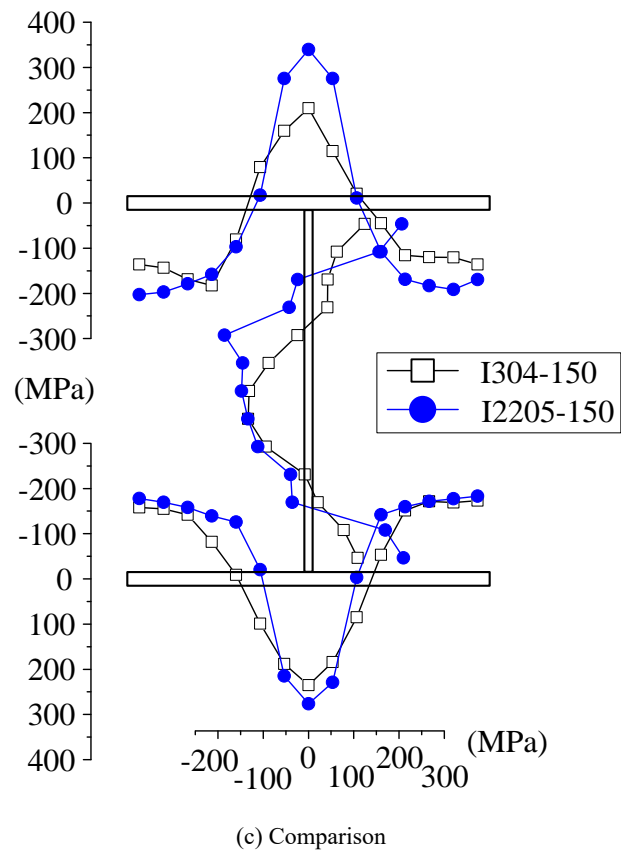
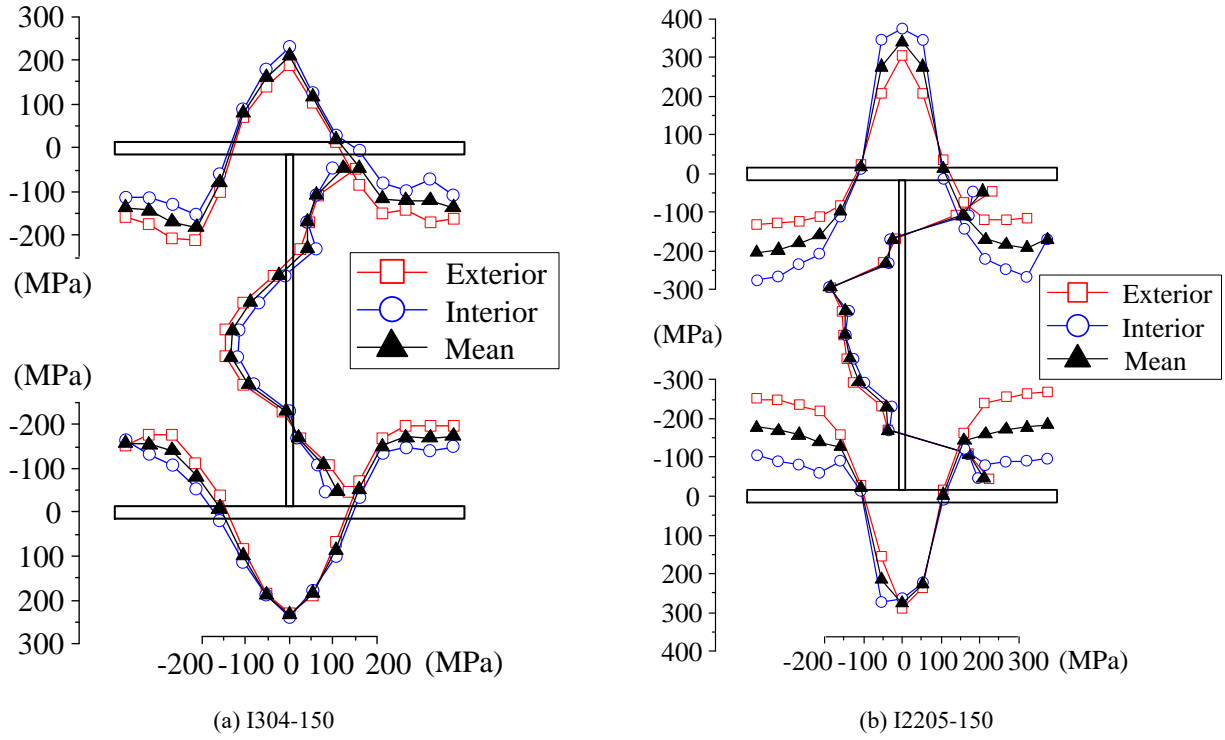


Fig.4. Residual stress distribution in specimens I304-150 and I2205-150

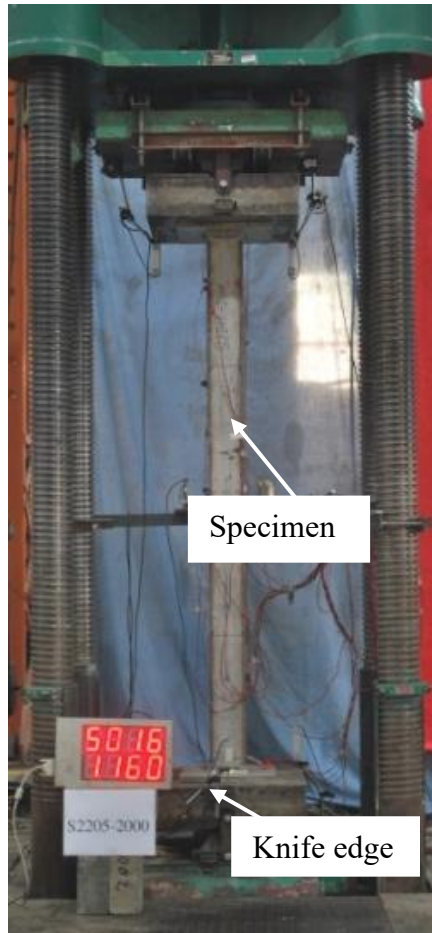
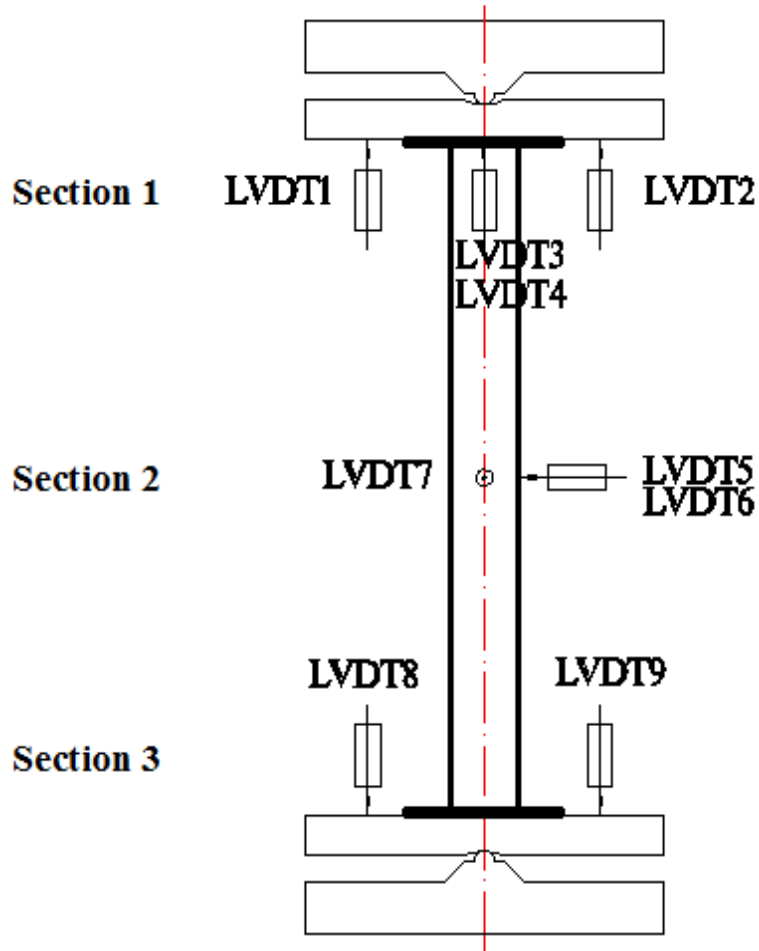
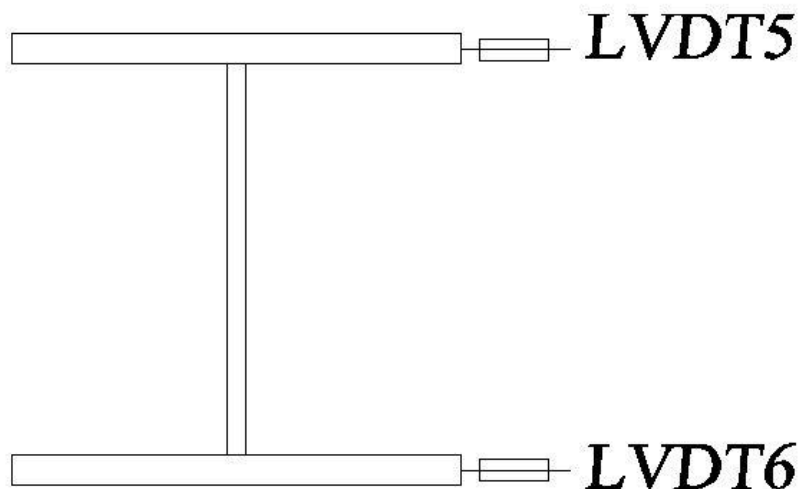


Fig.5. Test configuration

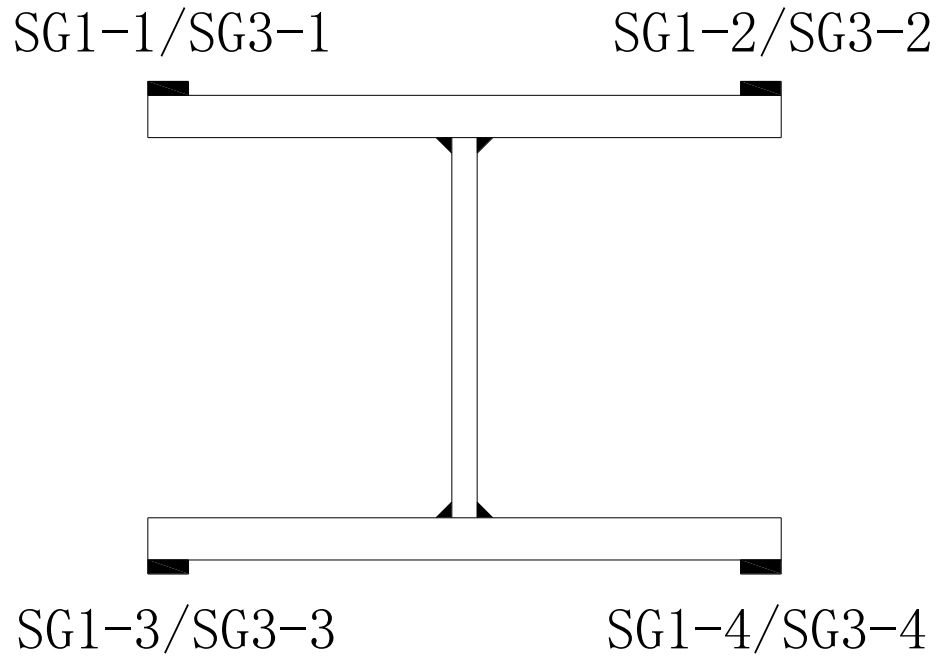


(a) LVDT arrangement

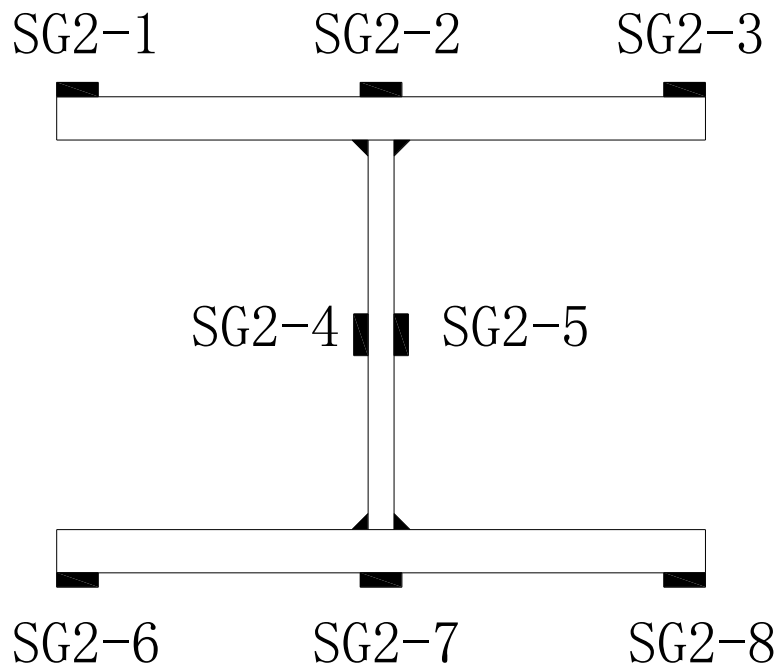


(b) Detail of section 2

Fig.6. Displacement transducer setup



(a) At end of column (Section 1 and Section 3)



(b) At mid-length of column (Section 2)

Fig.7. Strain gauge layout

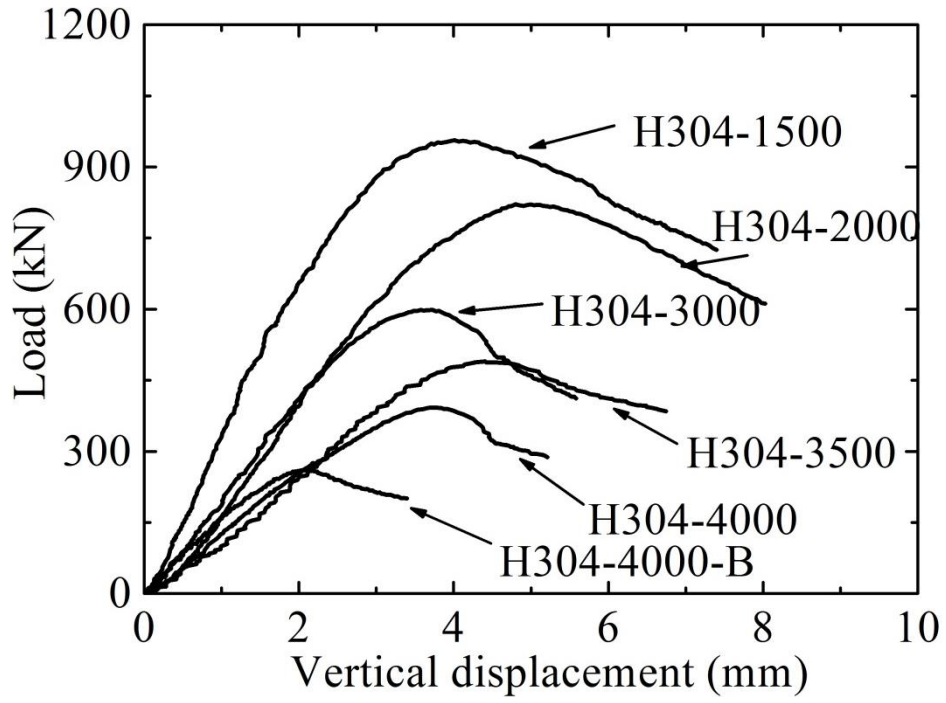


(a) I304-2000

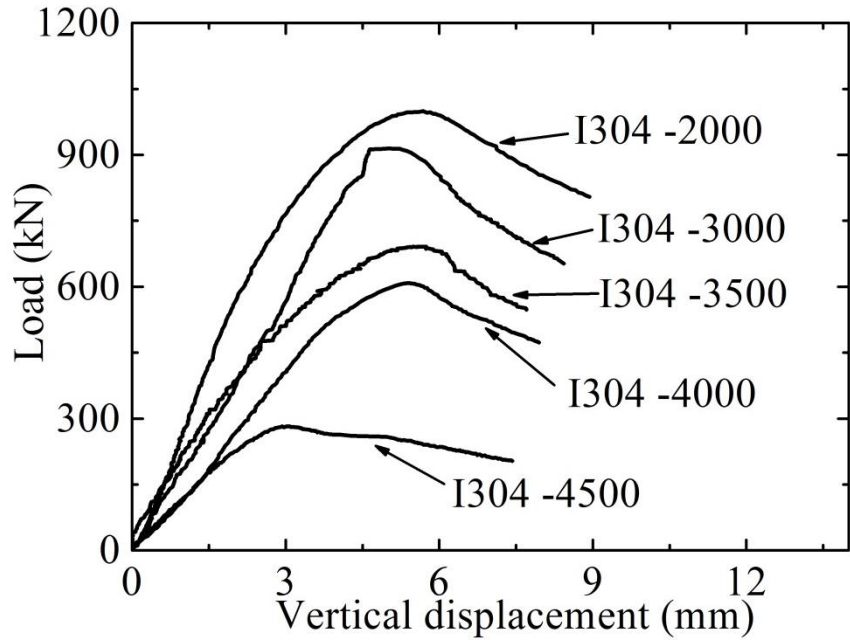


(b) I2205-2000

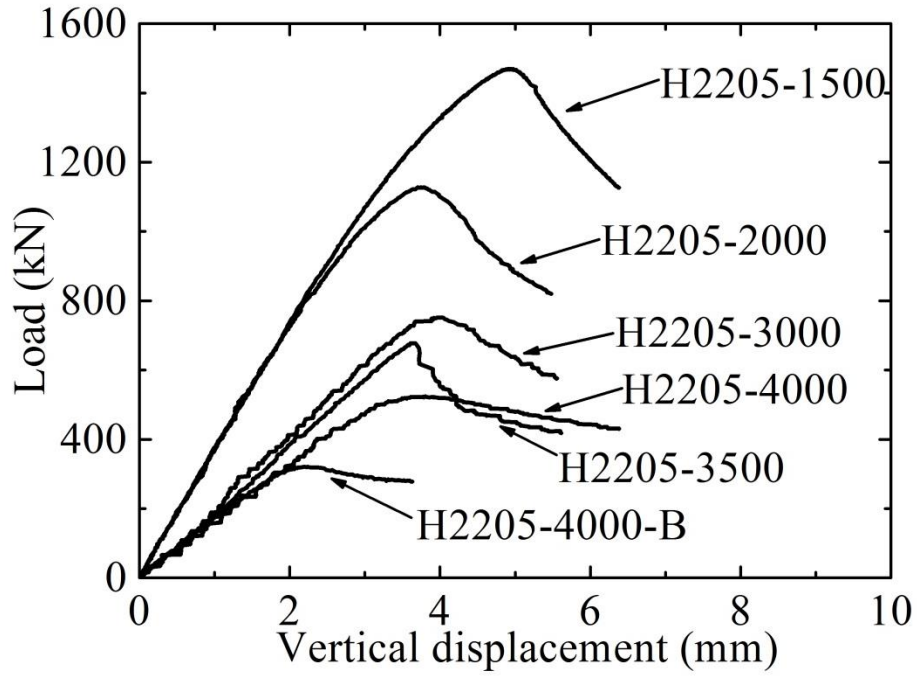
Fig.8. Typical buckling modes



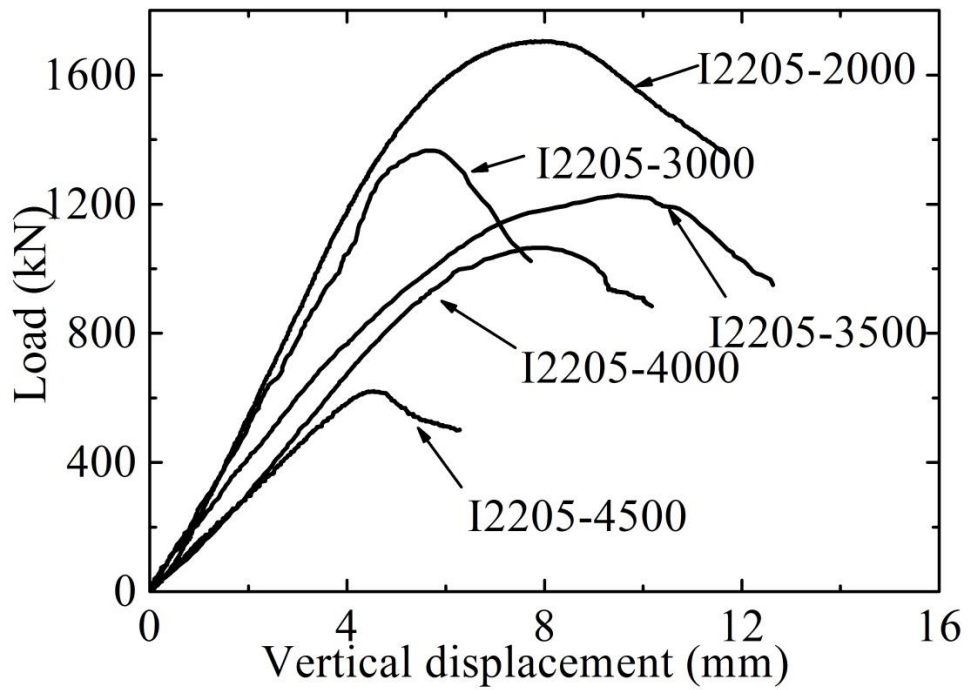
(a) H304



(b) I304

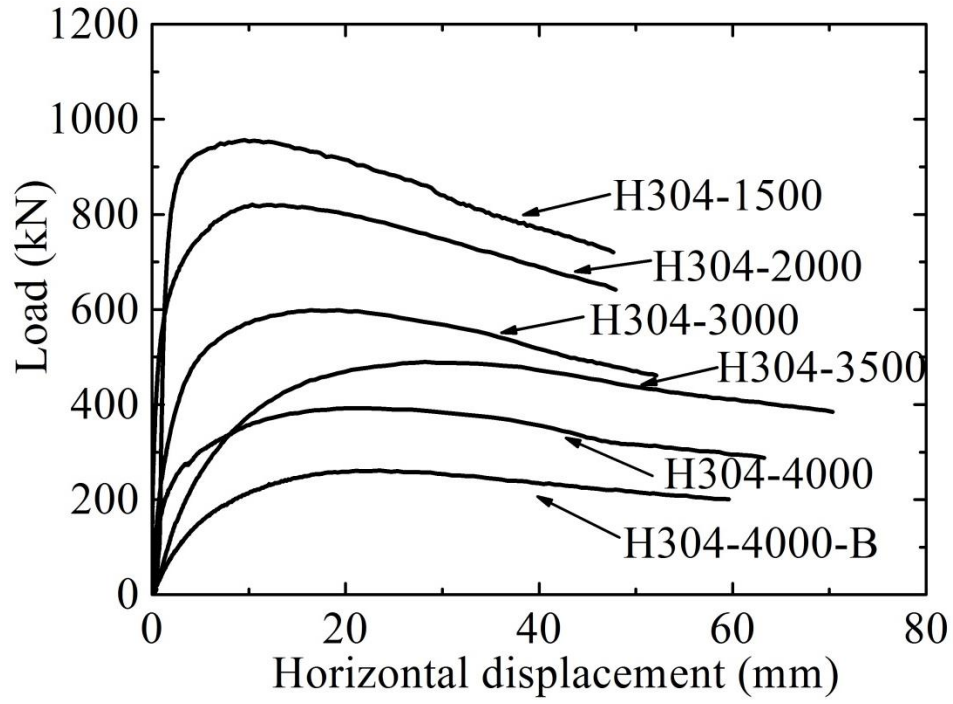


(c) H2205

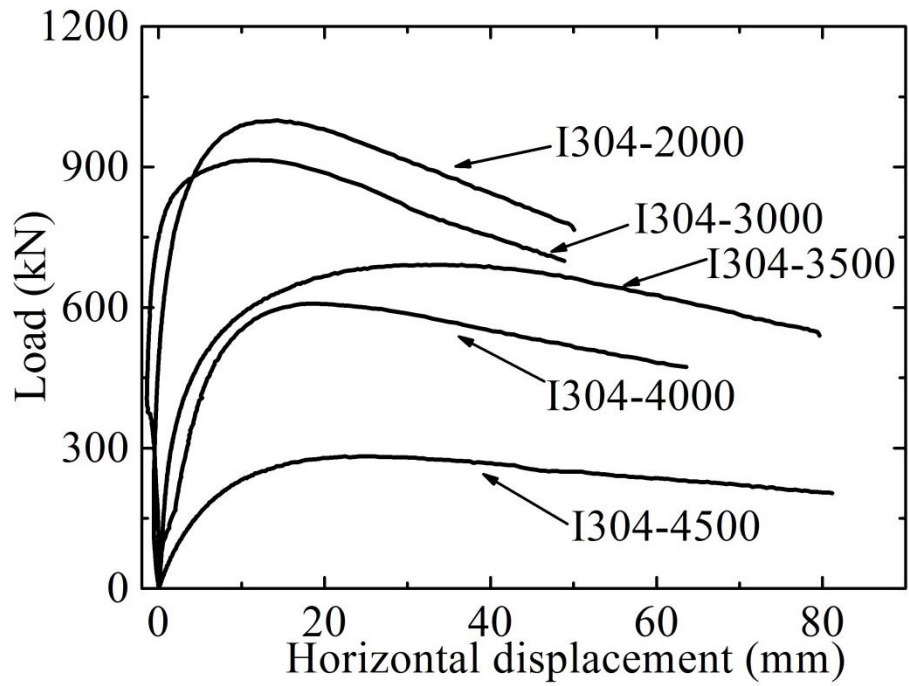


(d) I2205

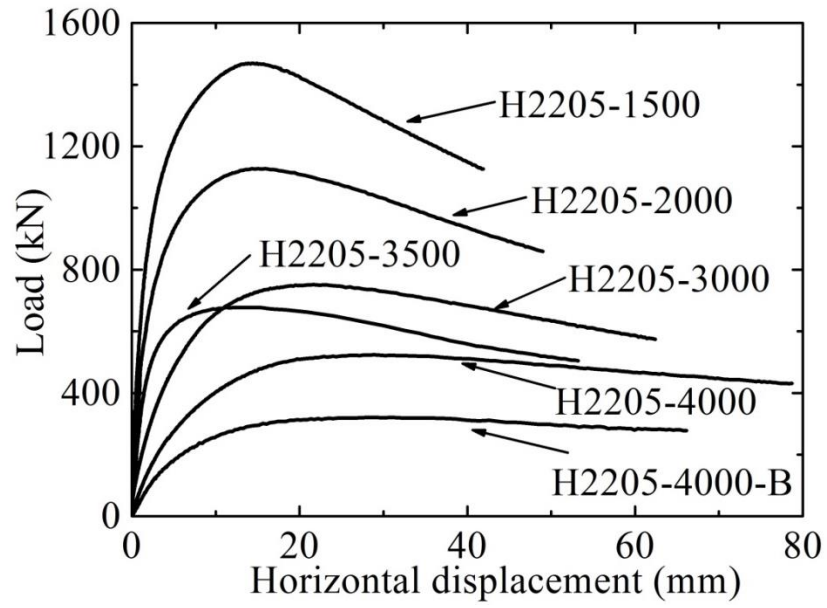
Fig. 9. Load- vertical displacement curves



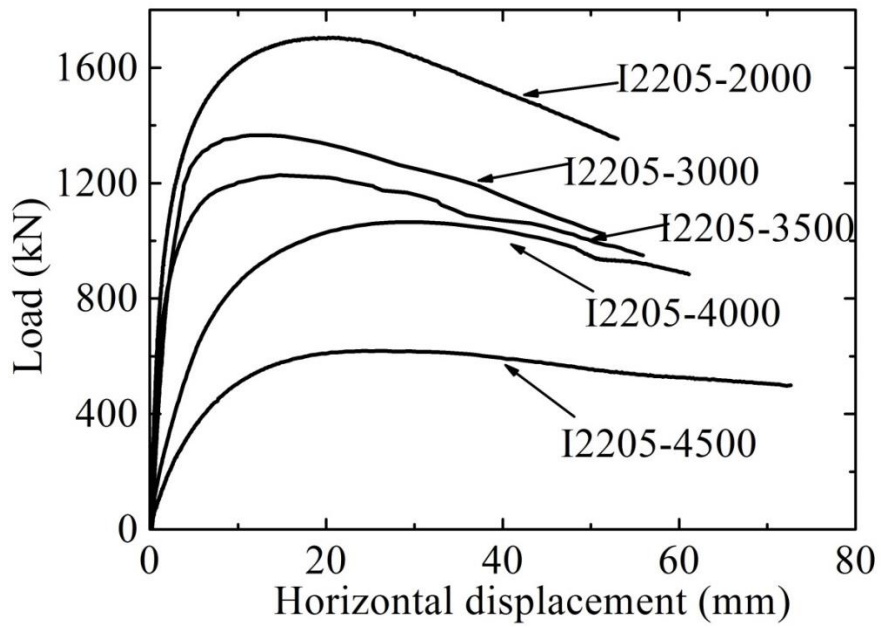
(a) H304



(b) I304

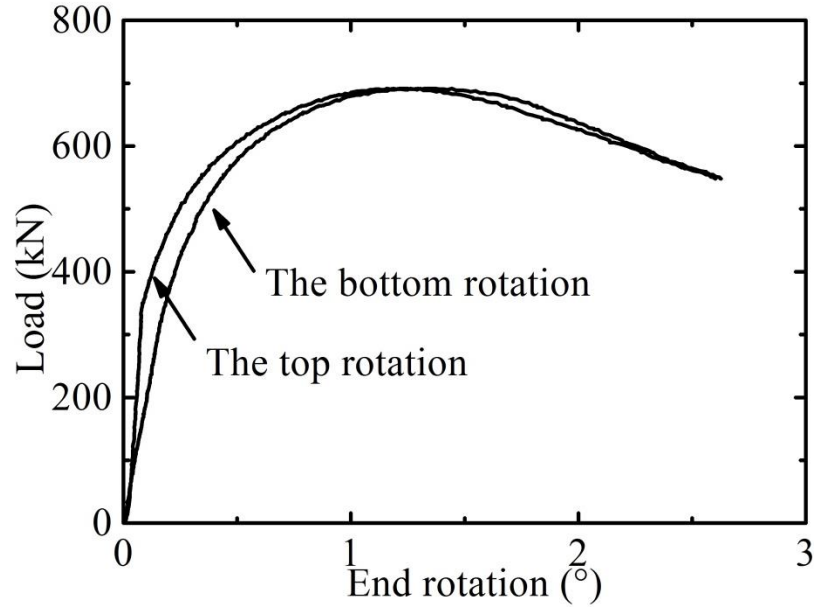


(c) H2205

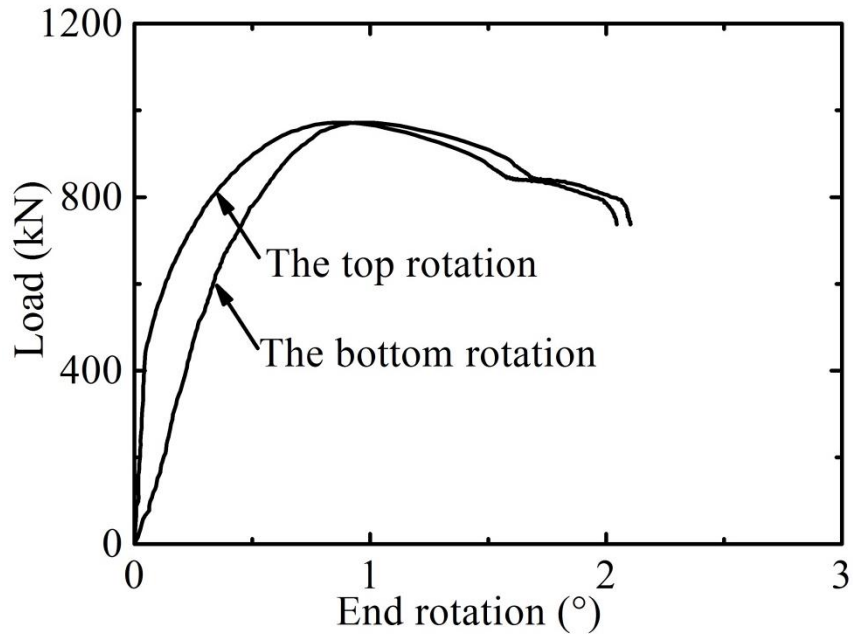


(d) I2205

Fig. 10. Load- horizonal displacement curves

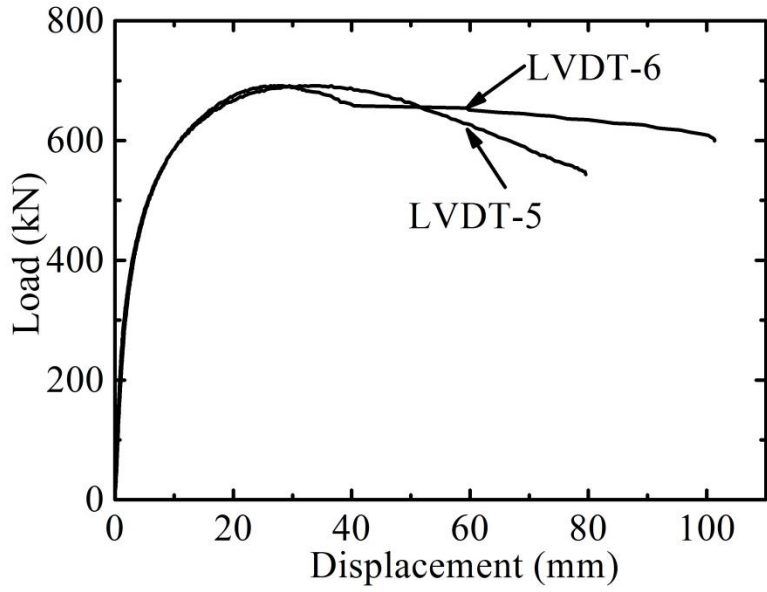


(a) I304-4000

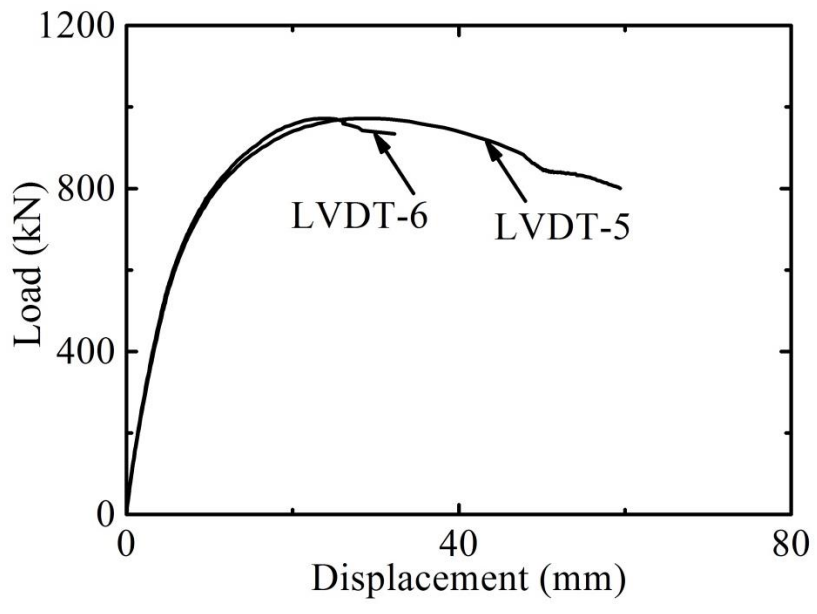


(b) I2205-4000

Fig. 11. Load-end rotation curves

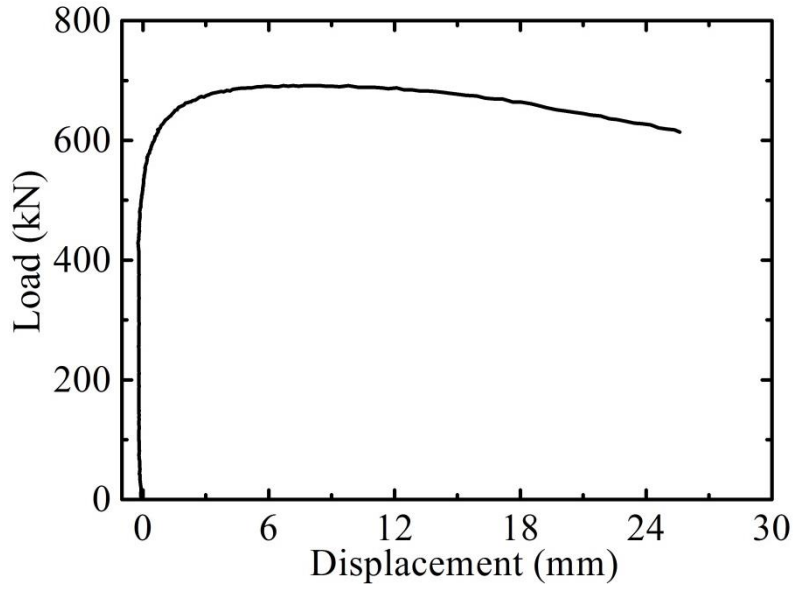


(a) I304-4000

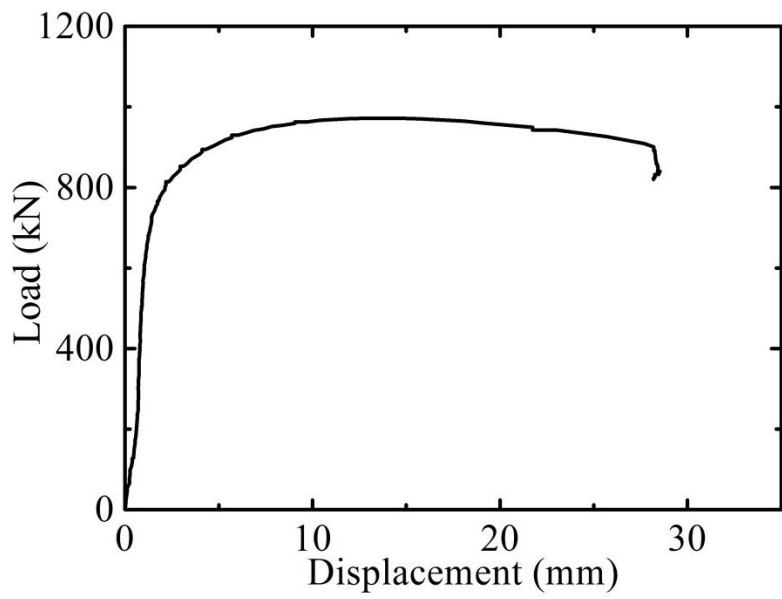


(b) I2205-4000

Fig. 12. Load- in-plane displacement curves

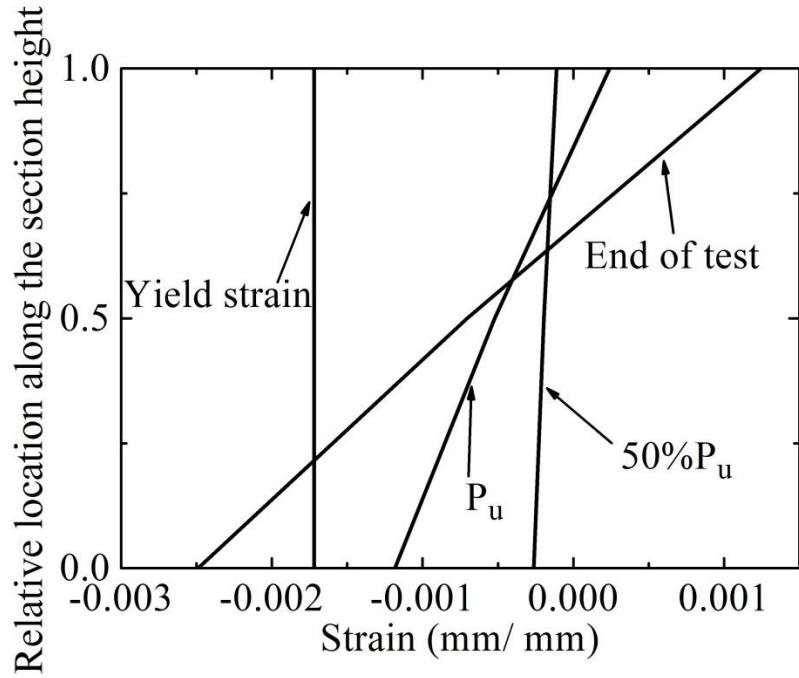


(a) I304-4000

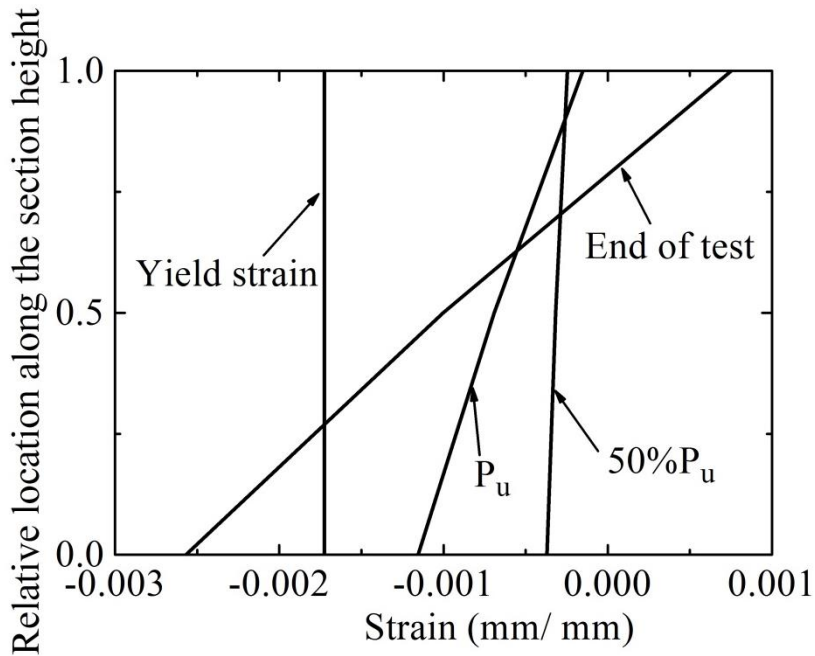


(b) I2205-4000

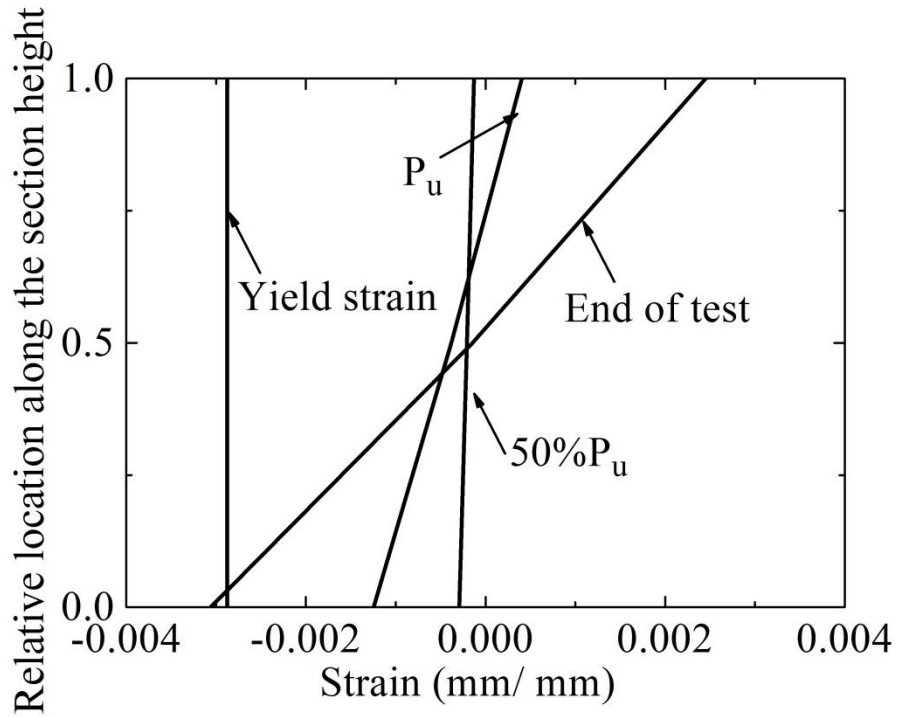
Fig. 13. Load-out of plane displacement curves



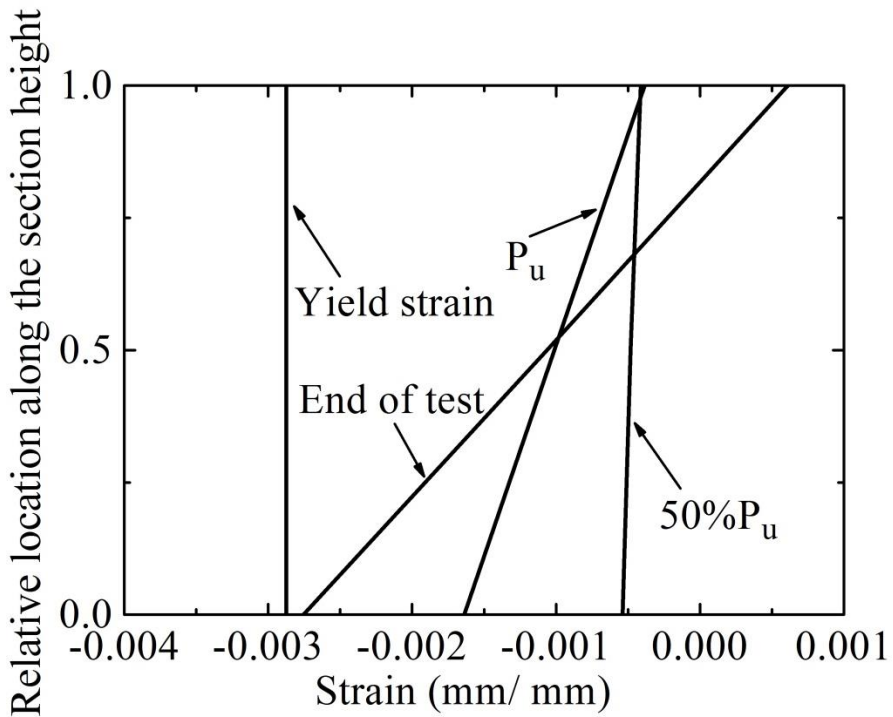
(a) H304-4000-B



(b) I304-4500

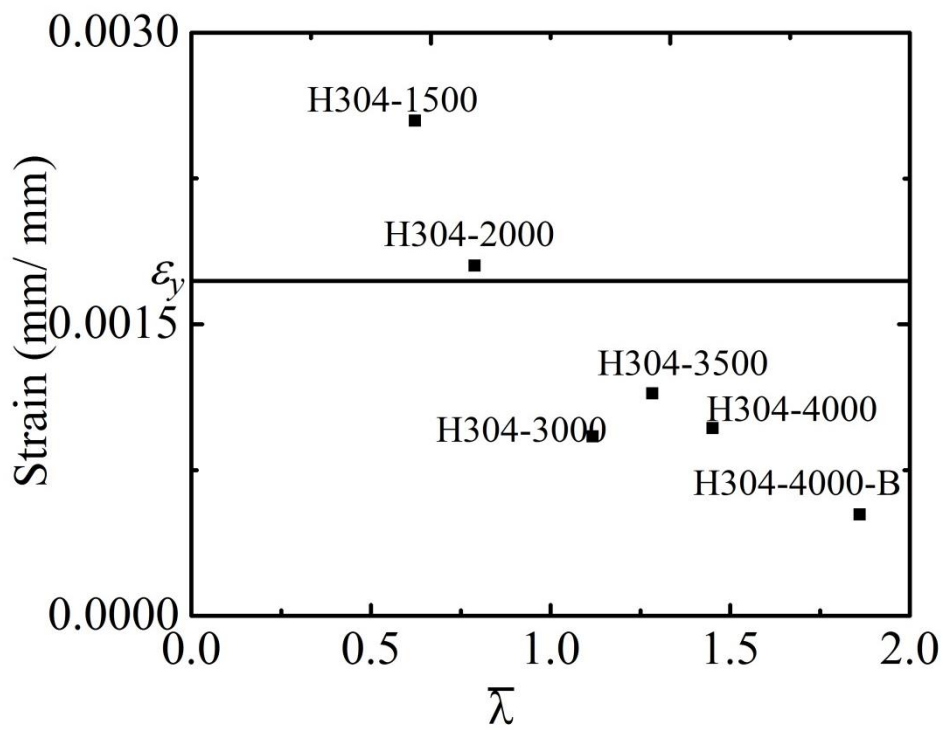


(c) H2205-4000-B

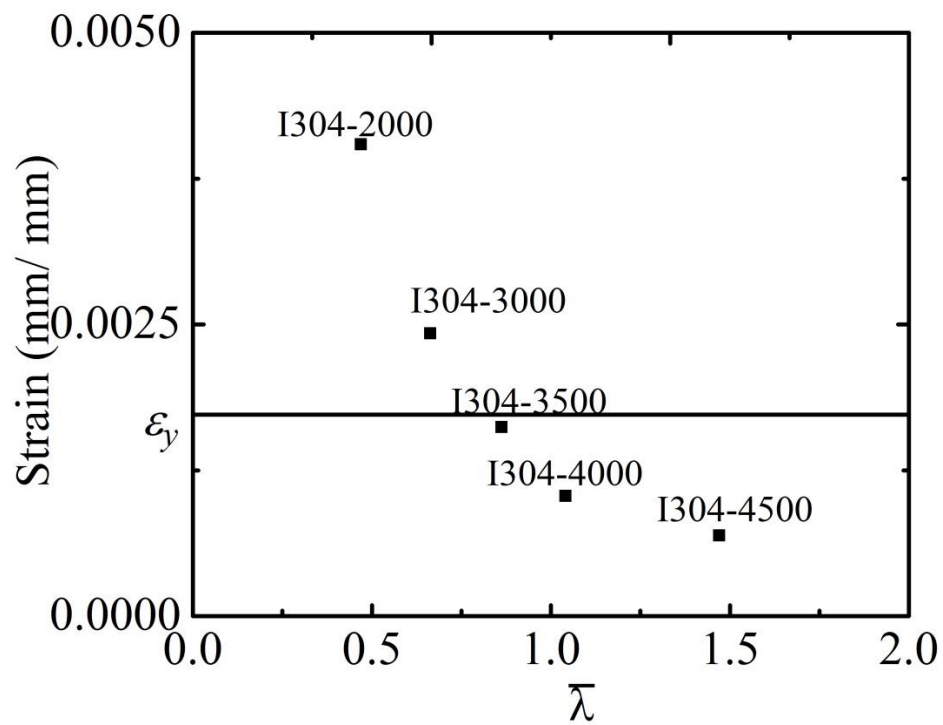


(d) I2205-4500

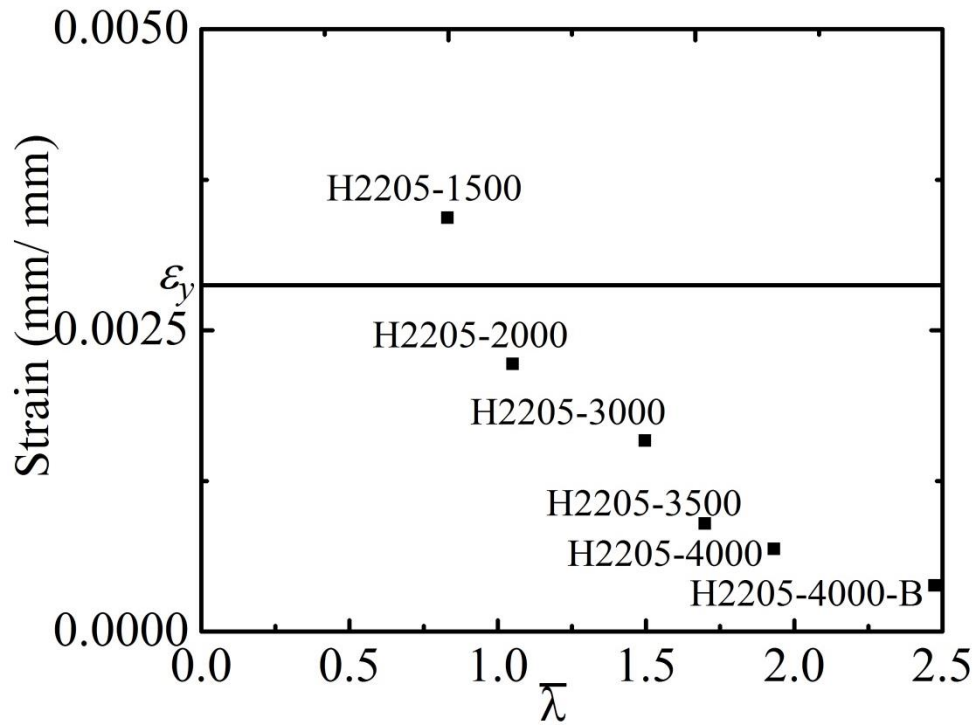
Fig.14. Strain distribution and development of column sections



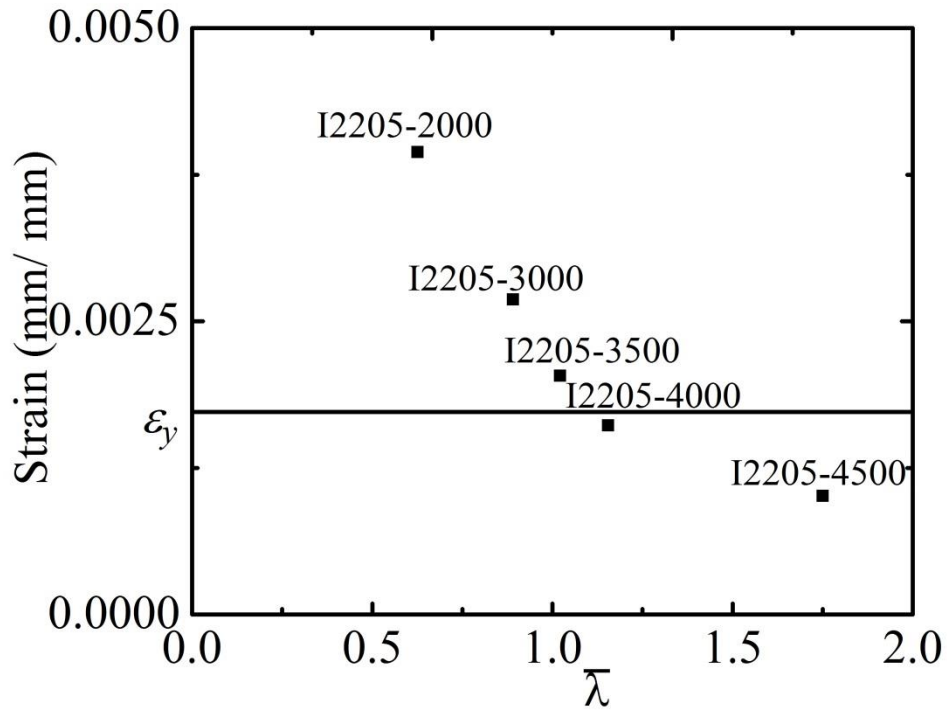
(a) H304



(b) I304

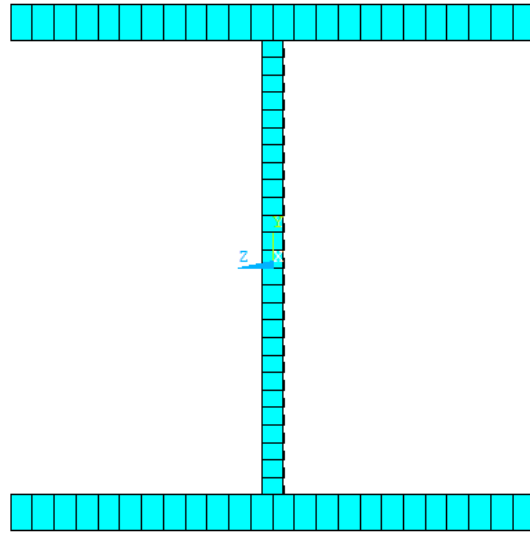


(c) H2205

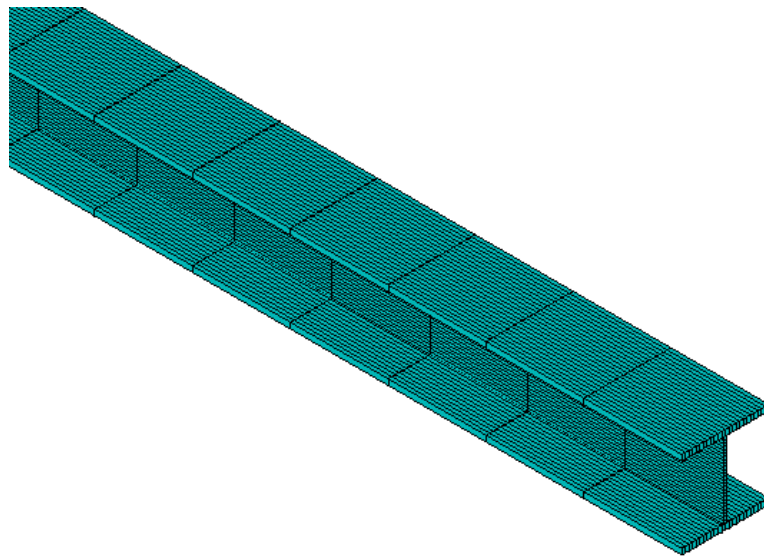


(d) I2205

Fig.15. Strain in mid-length section at overall buckling

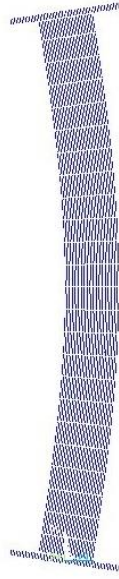


(a) Side view

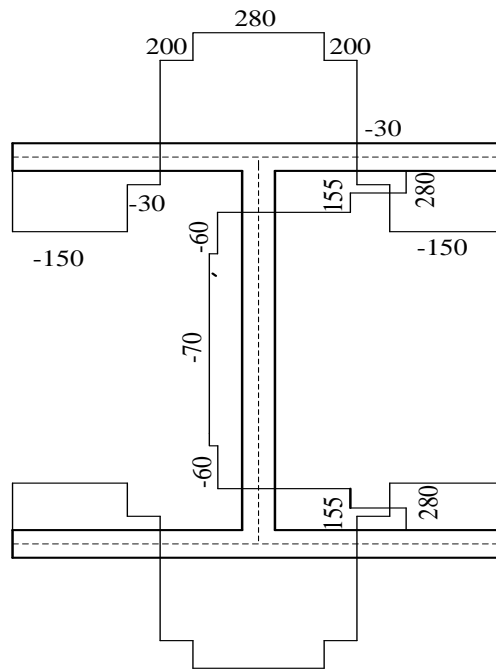


(b) 3-D view

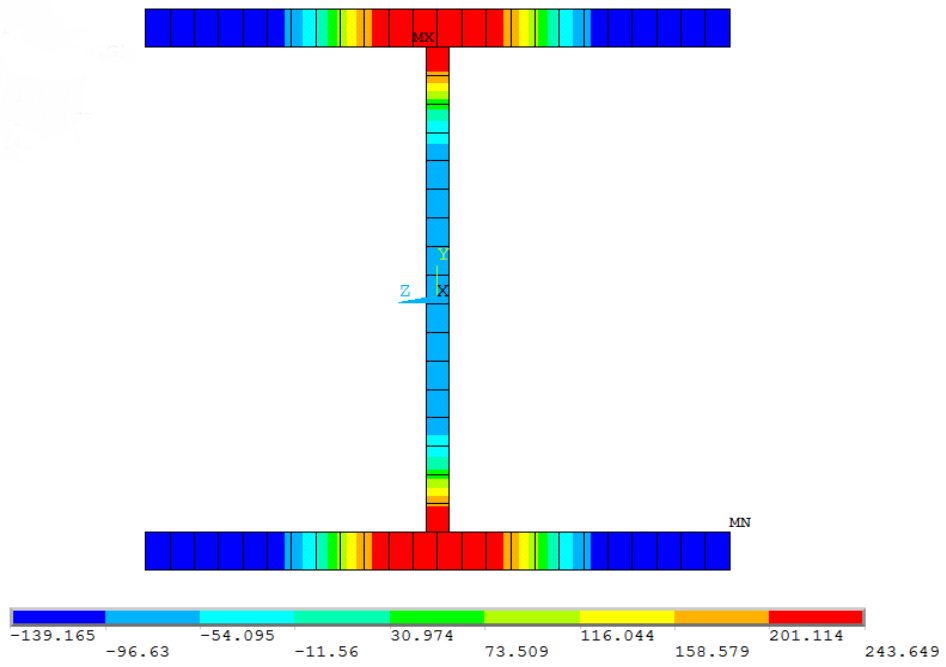
Fig. 16. The mesh of FEA model



(a) The amplified initial column buckling mode

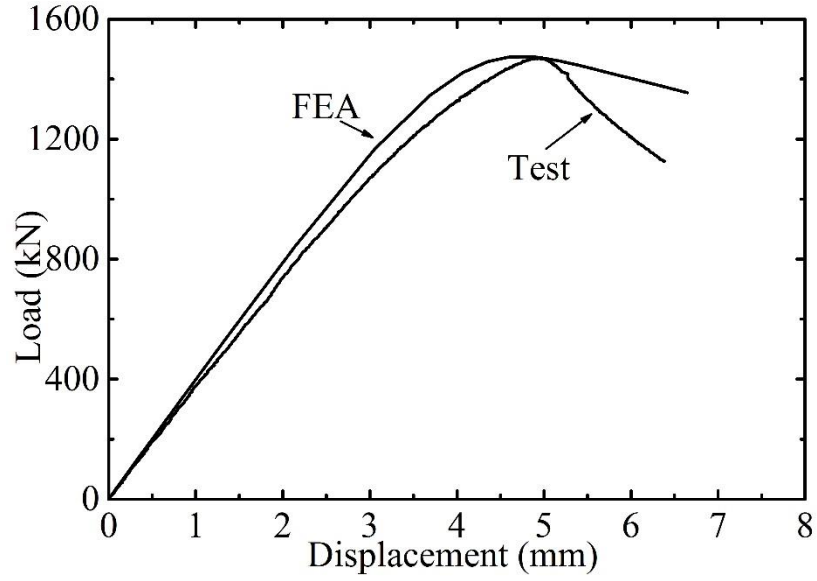


(b) Simplified residual stress distribution

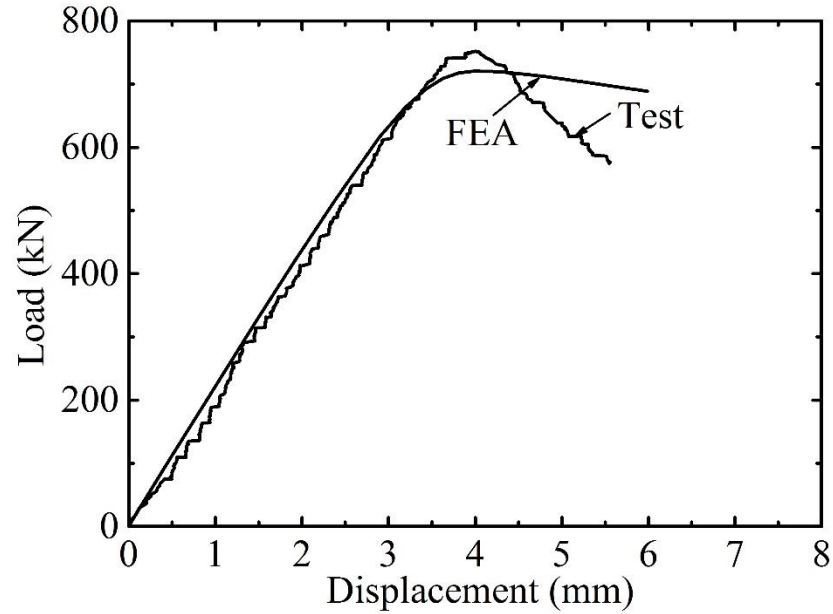


(c) Simulated residual stress

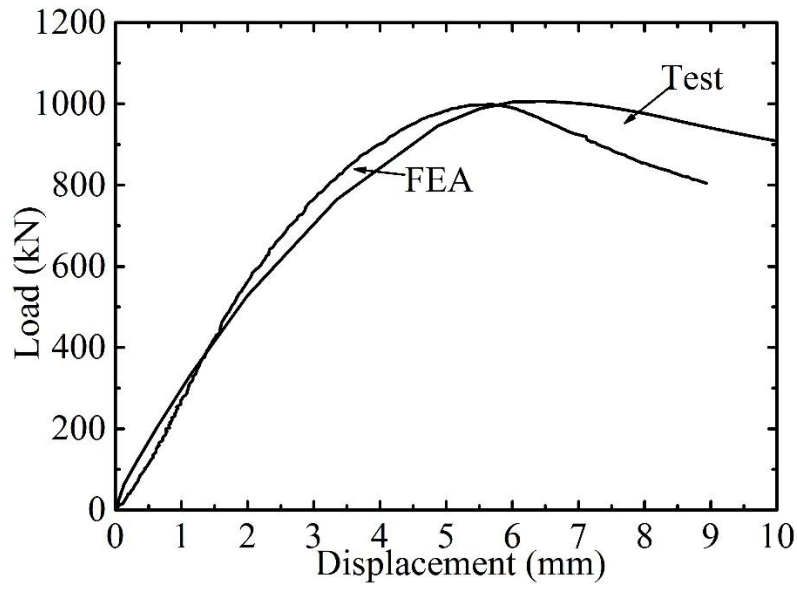
Fig.17. Residual stress distribution



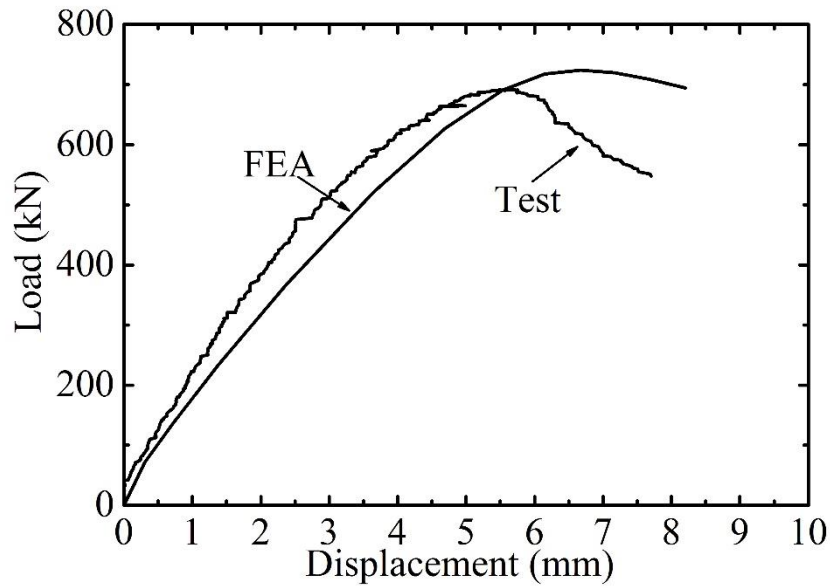
(a) H2205-1500



(b) H2205-3000

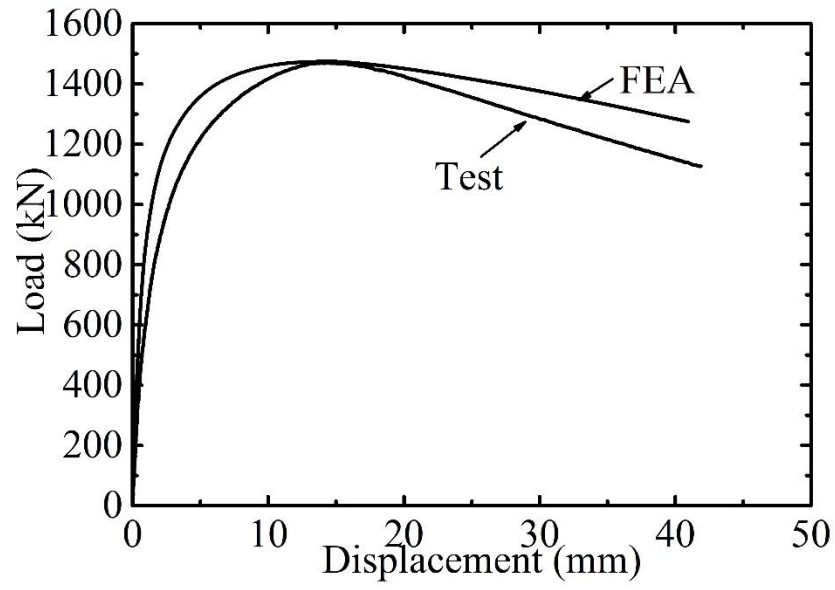


(c) I304-2000

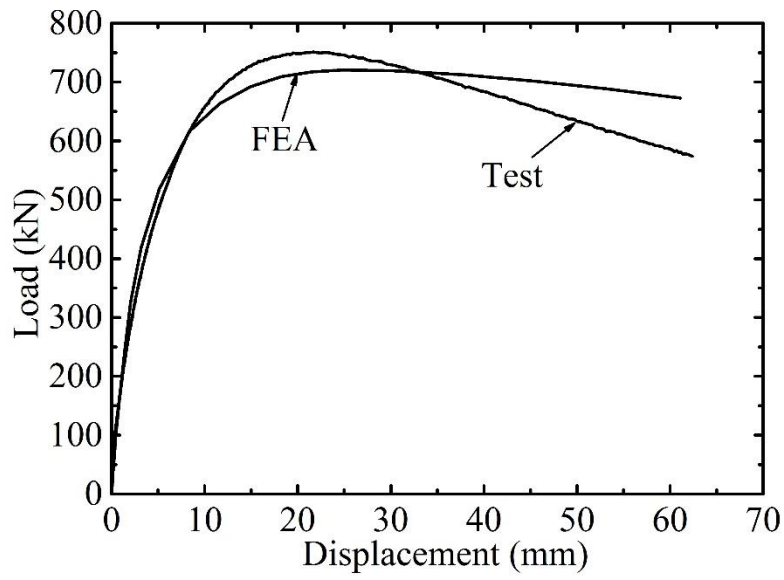


(b) I304-4000

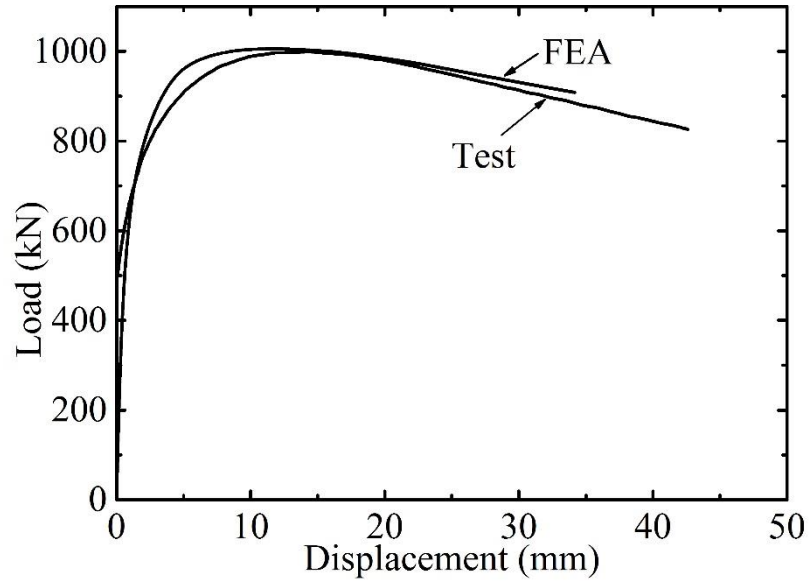
Fig.18. Experimental and numerical load–vertical displacement curves



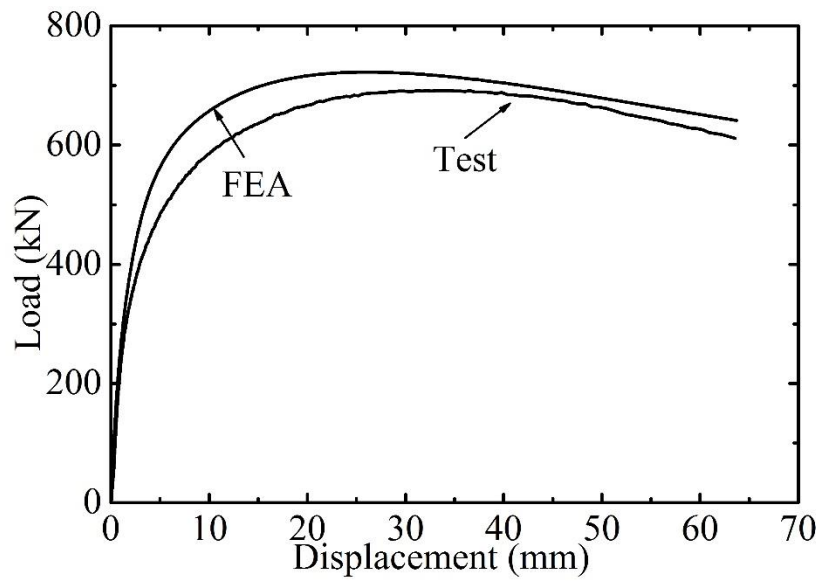
(a) H2205-1500



(b) H2205-3000

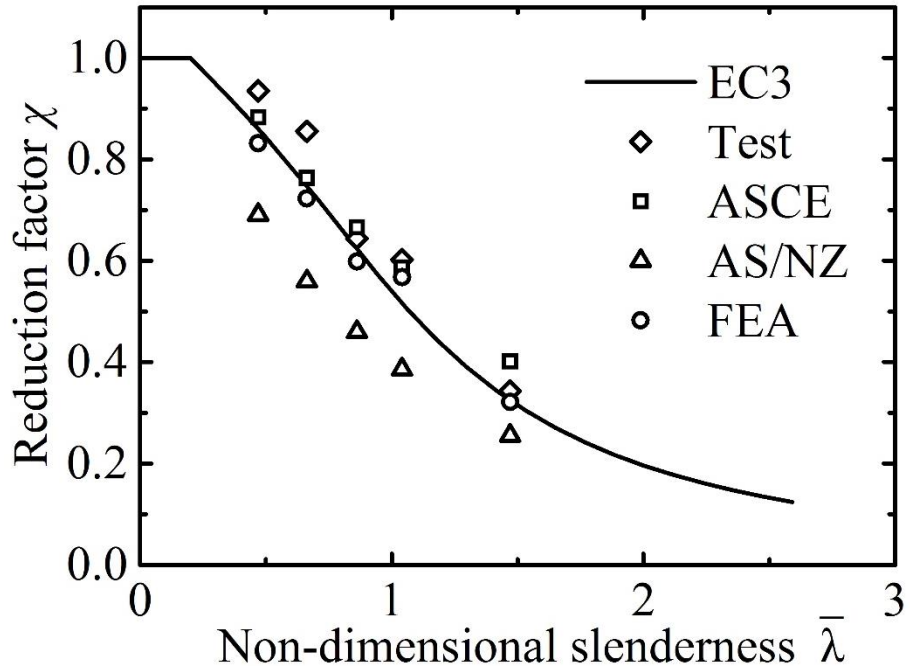


(c) I304-2000

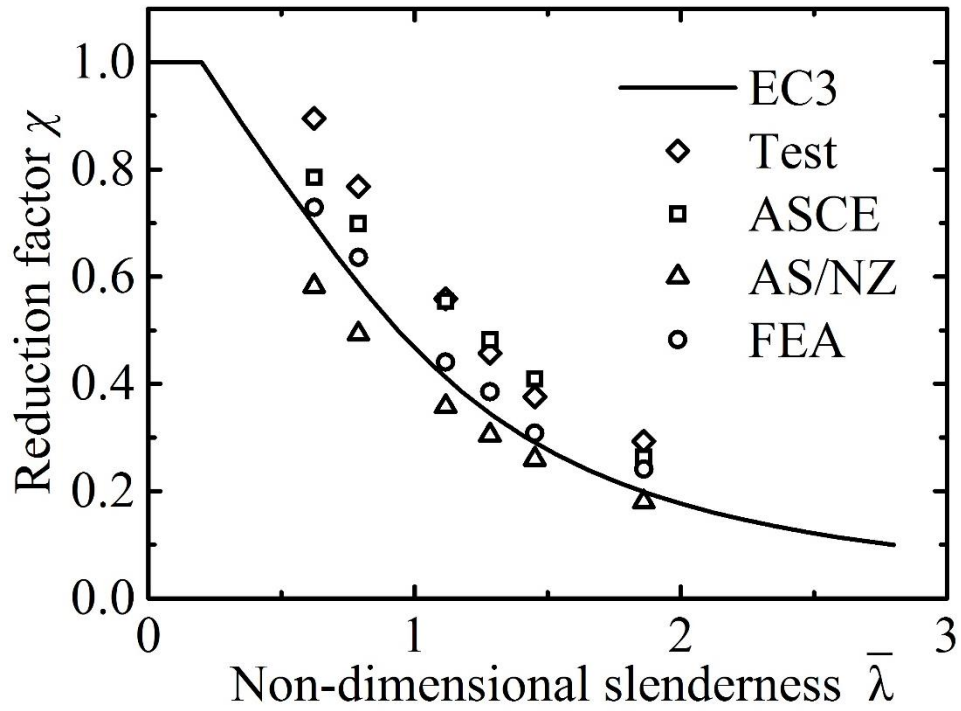


(d) I304-4000

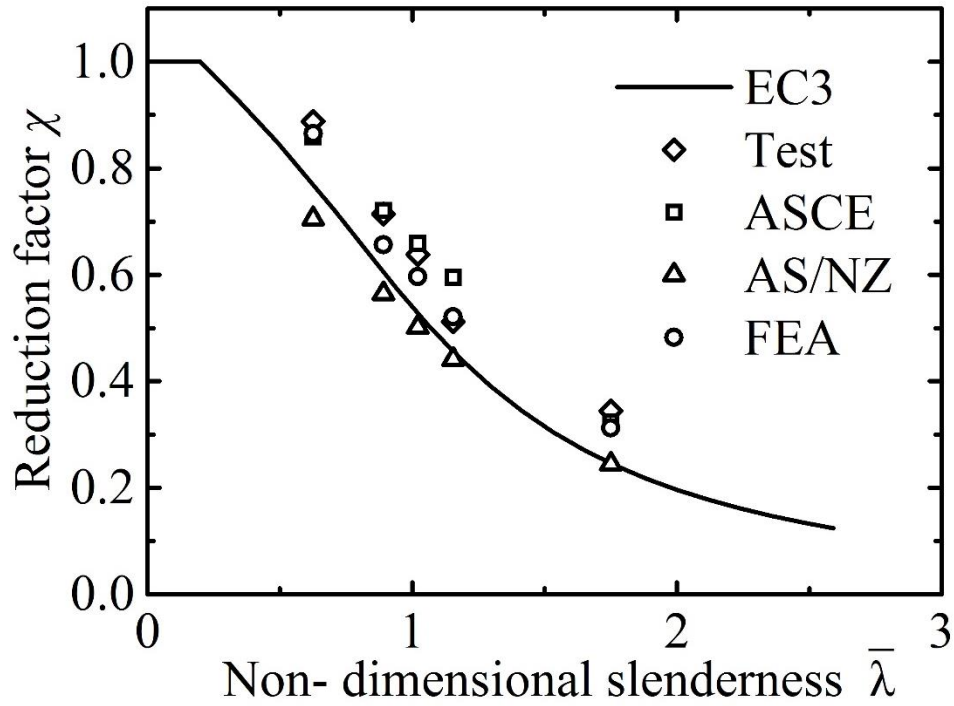
Fig.19. Experimental and numerical load–lateral displacement curves



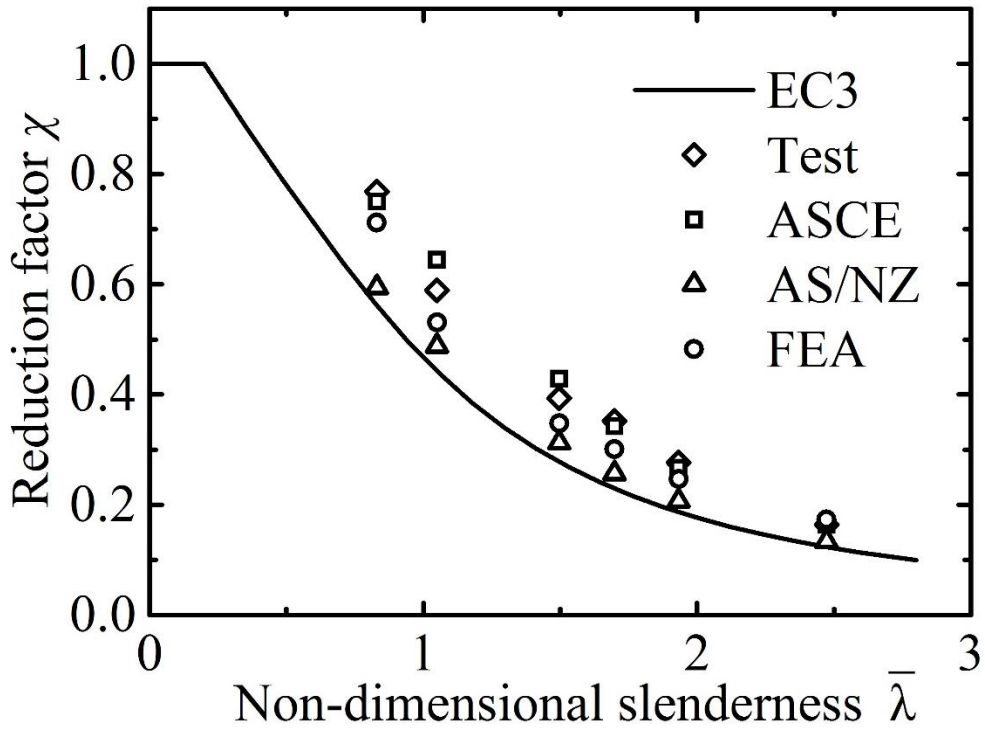
(a) I304



(b) H304



(c) I2205



(d) H2205

Fig.20. Comparisons of experimental results with specification predictions